Sensors & Diagnostics

ROYAL SOCIETY OF CHEMISTRY

CRITICAL REVIEW

View Article Online
View Journal | View Issue

Cite this: *Sens. Diagn.*, 2022, **1**, 648

Advances in integrated digital microfluidic platforms for point-of-care diagnosis: a review

Yuqian Zhang [ab] and Yuguang Liu [*abc]

Received 23rd February 2022,
Accepted 27th April 2022

DOI: 10.1039/d2sd00031h

rsc.li/sensors

Prompt, reliable and specific detection techniques in portable and easy-to-operate systems are of paramount importance to medical diagnosis, especially in emergencies such as pandemic outbreaks or in resource-limited settings. Point-of-care (POC) testing platforms can offer accurate screening in a timely manner, making these tools ideal under these circumstances. Digital microfluidics (DMF) is a fluid handling technology that enables programmable manipulation of discrete droplets (picoliter to microliter range) on a planar surface featured with electrodes, by changing the surface tension of droplets using electric fields. This technology allows user-defined droplet manipulation such as dispensing, mixing, splitting and merging, and thus the platform can be reconfigured for various assays. Although efforts have been undertaken to optimize the accuracy of fluid handling in DMF devices, implementing these devices for POC testing requires the integration of various detection techniques for on-chip assays. In this review, we highlight recent advancements in the integration of analytical tools into DMF devices, and discuss the current challenges and potential solutions as well as future outlooks for an automated, integrative platform for POC applications.

1. Introduction

Point-of-care (POC) is one of the most promising concepts in medical diagnosis, as it provides essential information for effective treatments in a rapid and convenient manner.[1] Ideal POC devices usually integrate sample pre-treatment, analyte separation and detection in a single platform for result analysis. Microfluidics, in recent decades, has been extensively studied as a promising candidate for POC applications due to its potential of integrating multiple functions in a single device that can be used outside of the laboratory in minimally trained hands.[2,3] In addition, microfluidic systems have the ability to handle significantly reduced fluid volumes, high reaction efficiency and sensitivity compared with conventional methods. These intrinsic advantages make microfluidics ideal for biomedical applications in diagnosis and therapeutics. Continuous flow-based devices are the most common types in microfluidics, however, most of them require mechanical components specifically designed based on applications, and these components typically rely on external experimental setups such as pumps and pneumatic control systems to operate.[4] Besides, laborious design–fabrication–testing cycles are needed to build a specific device to suit different applications. Moreover, in some cases, tens or hundreds of microliter sample volume requisite in continuous flow-based microfluidic devices are still burdensome, such as in blood tests for pediatrics and neonates.

To circumvent those limitations, digital microfluidic (DMF) systems have emerged as a new candidate for POC applications. DMF is an electrowetting-based liquid-handling technology that can manipulate discrete microdroplets on an array of electrodes including droplet dispensing from a reservoir, moving, splitting and merging.[5–10] Compared with conventional continuous microfluidic platforms, these devices further reduce the sample volume to the nano- to pico-liter range[11–13] and can manipulate samples automatedly with minimal external modules. Moreover, a single DMF platform can be easily reconfigured for different applications, and is user-programmable, presenting an attractive, automated platform for POC applications.

Currently, DMF platforms have been utilized for on-chip sample preparations[6,11,14,15] including DNA library preparation[16–20] and protein separation to advance toward the automation of laboratory processes.[21] Based on these, commercial efforts have been focused on developing fully automated DNA library preparation systems such as VolTRAX (Oxford Nanopore Technologies, Oxford, UK) and NeoPrep System (Illumina, San Diego, CA) for downstream DNA

[a] *Department of Surgery, Division of Surgical Research, Mayo Clinic, Rochester, MN, 55905, USA. E-mail: Zhang.yuqian@mayo.edu*
[b] *Microbiome Program, Center for Individualized Medicine, Mayo Clinic, Rochester, MN, 55905, USA. E-mail: Liu.yuguang@mayo.edu*
[c] *Department of Immunology, Mayo Clinic, Rochester, MN, 55905, USA*

sequencing.[22,23] The integration of diagnostic technologies was also explored for POC detection in recent years.[24] The integration combines sample preparation and subsequent detection on a single device, which greatly decreases cross contamination and the need for manual operations.[25] From 2017 to date, FDA has cleared a few DMF-based *in vitro* diagnostic platforms. Among these was the ePlex system (GenMark Diagnostics, Carlsbad, CA) which integrates sample extraction, PCR amplification and optical-based detection into a single cartridge to detect pathogenic DNA/RNA within 24 hours. This system has been adapted to identify multiple types of infectious agents such as respiratory pathogens,[26] bloodborne bacteria[27] and SARS-CoV-2.[28] SEEKER (Baebies, Durham, NC) is another FDA authorized DMF-based diagnostic platform used to screen newborns for lysosomal storage disorders (LSDs).[29] This platform offers multiple fully automated enzymatic assays on a single chip and completes screening within 3 hours. Although the commercialization of such platforms presents a promising role of DMF in POC diagnosis and clinic applications, the detection strategies are mostly limited to optical technologies, which rely on bulky and costly optical instrumentation typically used in laboratory settings. Therefore, the unmet need is the development of DMF-based platforms that are portable, automated and cost-effective for POC diagnostics; these platforms can bring rapid disease diagnosis and screening to various settings including emergency sites and resource-limited regions.

In this work, we review the state-of-art detection schemes integrated into DMF platforms to provide a comprehensive summary of such integrated systems adopted for the detection of biomolecules for POC testing. We mainly focus on DMF devices that use electrowetting-on-dielectric (EWOD) droplet actuation as it is the most commonly used mechanism in these platforms. Other droplet actuation technologies including surface acoustic wave,[30,31] dielectrophoresis[32,33] and magnetic forces[34,35] are reported elsewhere. Here, detection mechanisms in DMF platforms are categorized as optical, electrical, nuclear magnetic resonance and mass spectrometry, and we discuss each mechanism and their use in different applications including enzyme assays, immunoassays, cell-based assays and nucleic-acid based applications. We also discuss the limitations of on-chip detection and the selection of DMF substrates and future outlook for the potential applications of DMF platforms in POC diagnosis.

2. Digital microfluidics: principle of EWOD

Electrowetting-on-dielectric (EWOD) configures the electrowetting phenomenon on a dielectric substrate,[36] and is the most popular format in DMF, which has been adopted for various applications in biology and medicine.[37] Electrowetting was first discovered by Lippman in 1875,[38] which describes the phenomenon of conductive liquid spreading on an electrode surface directly under an applied electric field.[39] In 1993, Berge initiated EWOD, where a dielectric layer was added to separate the liquid and the electrode.[40] Although higher voltages are required, EWOD is preferred over direct electrowetting because it prevents electrolysis and allows for a stronger electrowetting effect before an electrical breakdown; on top of the dielectric layer, an additional coating of a hydrophobic layer can ease droplet movement. In EWOD, when a droplet of conductive fluid is positioned on an electrode covered with a hydrophobic and a dielectric layer, it adopts a spherical cap shape in its mechanical equilibrium; as an electric potential is applied to the electrode, a layer of charge builds up at the droplet–insulator interface, leading to reduced interfacial tension and therefore contact angle (θ_V), as shown in Fig. 1A. The voltage-dependent contact angle is described by the Lippmann–Young equation (eqn (1)).[41–43]

$$\cos\theta(V) = \frac{\varepsilon_0\varepsilon_r V^2}{2\gamma d} + \cos\theta_0 \quad (1)$$

where θ_0 and $\theta(V)$ represent the contact angle before and after applying the electrical potential, ε_0 and ε_r depict the permittivity of free space and the relative permittivity of the dielectric layer, and d is the dielectric layer thickness. γ represents the interfacial tension between the conducting liquid (droplet) and the insulating medium. By switching the voltage "on" and "off" between adjacent electrodes, the interfacial tension gradient causes shear force to drive droplets.

EWOD usually has two configurations: single-plate (Fig. 1B) and two-plate (Fig. 1C). In single-plate (open) structure, a droplet is placed on a single substrate with actuation and ground electrodes (coated with dielectric and hydrophobic layers), while in two-plate (close) structure, a droplet sits between an actuation electrode on the bottom substrate (coated with dielectric and hydrophobic layers) and

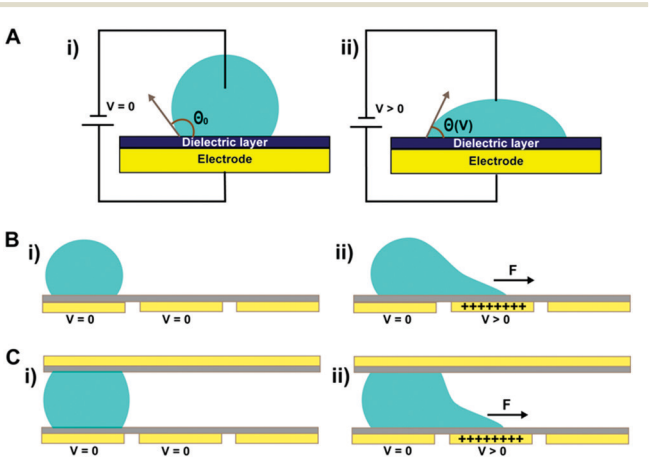

Fig. 1 (A) Schematic of electrowetting: droplet on an electrode coated with a dielectric layer without i) and with ii) electrical potential applied; droplet actuation in (B) a single-plate platform and (C) a two-plate platform without i) and with ii) electrical potential applied.

a ground electrode on the top substrate (coated with a hydrophobic layer). By patterning an electrode array on the substrate and switching the voltage "on" and "off" between a series of adjacent electrodes, the interfacial tension gradient causes shear force to drive droplets, likewise the droplet is able to move along the trace of the actuated electrodes. Both structures can move and merge droplets, but droplet splitting is only feasible in two-plate structure. A detailed review on electrowetting has been reported by Nelson *et al.*[44]

In the EWOD-device design, the device is mainly composed of four parts: substrates, electrodes, dielectric and hydrophobic layers. The electrodes are often metallic, such as platinum, chromium and gold, and are typically fabricated through photolithography on the bottom substrate. The dielectric layer is then deposited on the patterned electrodes through vapor deposition (*e.g.*, parylene) or spin-coating (*e.g.*, SU-8 photoresist). Lastly, a hydrophilic layer (*e.g.*, Teflon AF, fluoropolymer) is coated onto the surface. In the two-plate configuration, the top substrate is coated with an electrically conductive material to serve as the ground electrode, and also a hydrophobic layer. Indium tin oxide (ITO), as a transparent and conductive material, is typically used as the ground electrode on the top substrate for better visualization of droplets.

3. In-line detection technologies integrated into DMF platforms

With the advent of EWOD, a variety of detection platforms have been implemented in DMF devices for analytical applications. Several attempts have been made to integrate analytical technologies into DMF platforms to detect biomolecules in a rapid and convenient manner. Recent advancements of integrating technologies including optical, electrical, nuclear magnetic resonance and mass spectrometry for on-chip biomolecule detection are discussed elaborately in this section.

3.1 Optical techniques

Optical biosensors are widely deployed for biomolecule detection owing to their superior sensitivity, reliability and reproducibility.[45,46] More often, these sensors require optical tags to label either the target or the biorecognition molecules, and the detection is indicated by the intensity of the optical signals. On the contrary, in label-free detection, the target molecules can be detected without additional tags, and the signals are often indicated by changes in reflection or wavelengths. Both strategies are implemented in DMF platforms, and their configurations are briefly illustrated in Fig. 2. Table 1 summarizes a number of representative configurations of DMF platforms with optical sensing capabilities reported in recent years, including their detection mechanisms, instrumentation, applications and limit of detection. The detection principles and their applications in DMF platforms are reviewed in the following section.

3.1.1 Label-based optical techniques

3.1.1.1 Fluorescence detection. Fluorescence detection is the most common optical biosensor format which uses well-established florescent-labeling techniques to achieve excellent detection sensitivity and selectivity. This format usually consists of an excitation light source to excite the fluorophore, and a fluorescent photodetector (*e.g.*, well-plate reader, microscope and spectrometer) to receive and process optical signals. Therefore, it can be implemented in a single or double plate DMF platform with transparent electrodes. Currently, these systems are being utilized to detect enzyme, proteins, cells and DNAs. It is worthwhile to mention that biofouling is still a main problem that hinders the expansion of various applications to DMF devices. To address this issue, pluronic additives (poly(ethylene oxide) poly(propylene oxide)–poly(ethylene oxide) (PEO–PPO–PEO), *e.g.*, Pluronic F68 and Pluronic F127) can be added in the droplets to relieve biofouling such as that caused by protein in immunoassays in DMF devices, since the poly(ethyleneoxide) (PEO) polymer can reduce non-specific surface adsorption of proteins and other molecules.[85,86] Another solution is to integrate a robust antifouling surface into DMF devices, such as a slippery liquid infused porous surface (SLPS).[87–90] This surface introduces the liquid–liquid contact between the droplet and lubricant liquid, thus diminishing the direct contact between the droplet and the solid interface and preventing non-specific adsorption of various biomolecules including proteins and DNA molecules onto the solid surface.

Enzyme-assay. Enzymatic assays are often used to identify the concentration of small enzyme molecules in biofluids. These assays usually rely on the catalyzed reactions of enzymes, which sometimes are challenged by the variation in conditions such as pH and temperature. Therefore, multiple measurements of enzymatic assays are needed to ensure the assay reproducibility. Enzymatic assays in DMF devices allow the dispense of samples and reagents in discrete droplets, presenting capability to test multiple microscale samples in parallel. Combined with fluorescence detection in a DMF device, enzymatic assays can be performed to detect, for example, alkaline phosphatase, with high sensitivity and efficiency.[47] In this homogenous assay, droplets that contain alkaline phosphatase and fluorescein diphosphate solutions were dispensed on-chip and thoroughly mixed in a rapid manner, which overcame the limitations of diffusional mixing in enzymatic assay channel-based microfluidic devices.[91] The DMF device was then inserted into a commercial multi-well plate reader for fluorescence reading in real-time to monitor the kinetic constant of the reaction under varying experimental conditions. The combination of DMF and fluorescence detection platforms provided a closer optical path between the device and the reader, thus improving detection sensitivity by two orders of magnitude and reducing sample volumes by 2.5 orders of magnitude compared with the conventional plate assay. This integrated system presented the capability to deliver enzymatic assays in a variety of

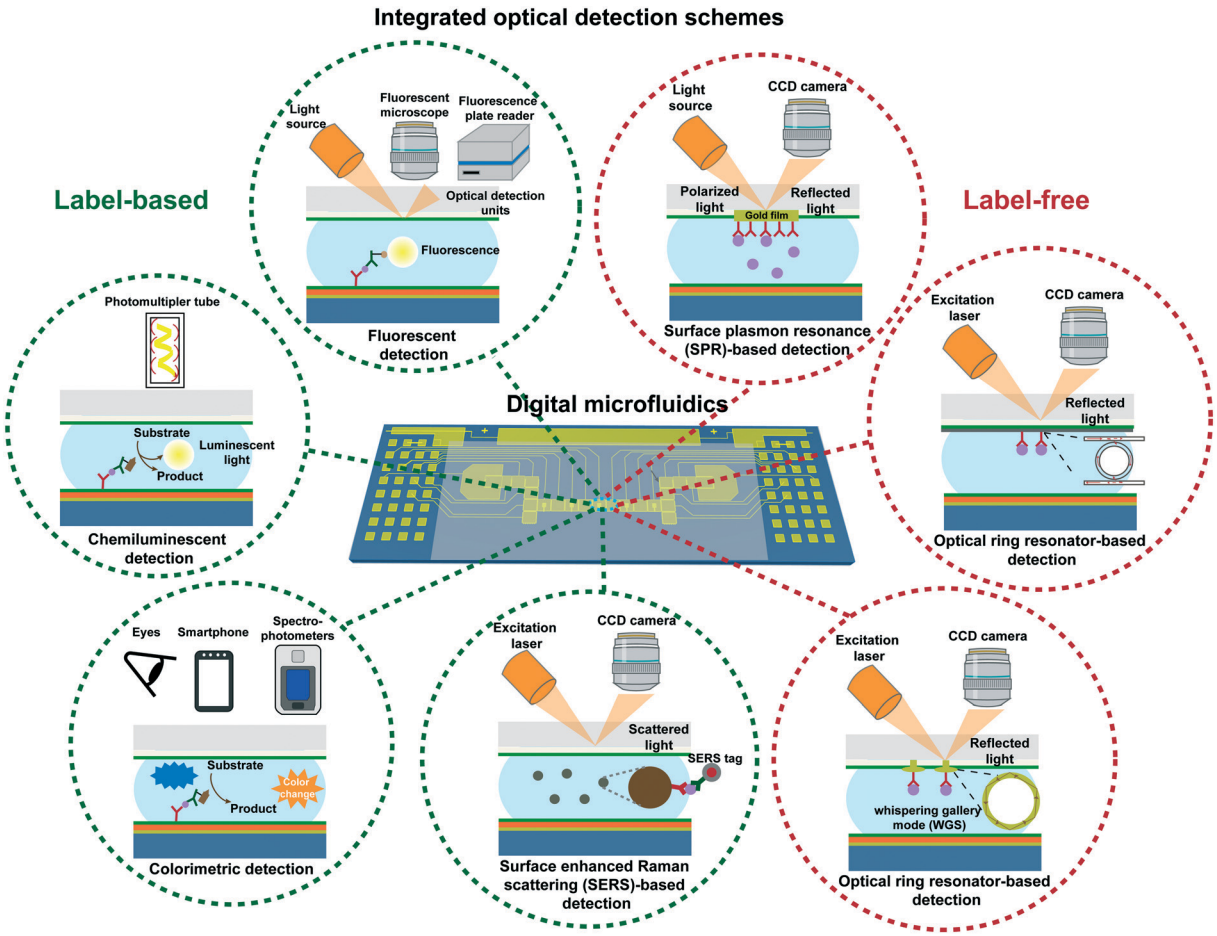

Fig. 2 Representative diagrams showing DMF platforms integrated with different label-based and label-free optical detection schemes.

biochemical analyses on the microscale, such as glucose monitoring in blood and enzyme inhibitor screening in pharmaceutical research.

Immunoassay. In immunoaffinity-based biomolecule detection, the immobilization of a biorecognition layer is required to capture target molecules at desired sites in DMF platforms. This can be achieved by using microspheres as solid supports to recognize targets in a sandwich assay (indirect binding) or immobilizing the targets on a surface functionalized with bio-recognition agents (direct binding). Among microspheres, micron/nano-sized magnetic beads are more widely used as solid assay carriers in fluorescence[48] or chemiluminescence detection,[62,63] owing to their high surface to volume ratio so that there are more binding sites for targets and thus the fluorescent markers. In addition, the beads can be manipulated independently (*e.g.*, aggregation and re-suspension) to enhance sample washing efficiency which is vital to reduce background signals. In this regime, Vergauwe *et al.* integrated a superparamagnetic nanoparticle (15 nm)-based bioassay into a DMF device to detect human IgE.[48] This approach allows the magnetic beads to be retained by a permanent magnet while the unbounded molecules, especially the excessive fluorescent markers, are washed away by passing multiple droplets of wash buffer in a serial manner. This approach led to the highly sensitive detection of target IgE as low as 150 nM.

Although the use of beads allows sensitive detection of proteins in DMF devices, it requires external magnets during the operation, and therefore involves extra manual intervention and complicates device design. An alternative strategy is to directly functionalize recognition molecules on the device surface for targets and fluorescent markers. Similarly, excessive fluorescent markers can be washed away by moving a series of droplets across the electrode immobilized with targets. However, device fabrication can be laborious due to the additional steps of surface modification, and the antibody-coated surface is hydrophilic which can interfere with droplet movement. One way to overcome these challenges is to immobilize capture antibodies on the top ITO substrate instead of the actuation electrode-configured bottom substrate, for several advantages: 1) the area of ground electrodes on the top substrate is relatively large, thus the smaller area of the hydrophilic antibody-coated surface can minimize the hindrance of droplet actuation; 2) the transparent top substrate can be detached from the device, which enables easy visualization in fluorescent readers, inverted or upright microscopy systems. 3) The top substrate can be replaced, therefore it is possible to re-use the bottom

Table 1 Optical-based sensing in DMF platforms for biochemical analytical applications

Detection principle	Instrumentation for integration	Applications	Results (LOD: limit of detection; DR: dynamic range)	Ref.
Fluorescence	Microplate reader	Homogeneous enzymatic assay to detect alkaline phosphatase	LOD: $\sim 7.0 \times 10^{-20}$ mol	47
	Fluorescence microscope	Enzymatic assay (glucose), magnetic bead (15 nm)-based immunoassay (lgE), MCF-7 cell and HeLa cell assays	DR: 26–150 mg L^{-1} (glucose); LOD: 150 nM (lgE)	48
	Microplate reader	T cell-based cytotoxicity assay	~20 time higher sensitivity than a conventional well plate assay	49
	Fluorescence microscope	Microalgal growth screening and different microalgal strain comparison	—	50
	Fluorescence microscope	A "cell invasion in digital microfluidic microgel system (CIMMS)" to analyze the cell invasion to a 3D extracellular matrix	—	51
	Microplate reader	Enzymatic endoglucanase assay and bacterial transformation performed in an automated reagent delivery DMF system containing a thermal control apparatus	—	52
	Microplate reader	Homogeneous sandwich assay to detect target protein (human IgG) in complex samples	DR: one-order-of-magnitude; high specificity: target human IgG can be detected in the presence of a 100-fold excess of bovine IgG	53
	Customized optical system including PMT and a fluorescence microscope	Programmable isothermal DNA amplification of antimicrobial resistance gene by recombinase polymerase amplification (RPA) within ~15 min	LOD: a single copy DNA DR: four-order-of-magnitude	54, 55
		Programmable amplification of multiple DNAs extracted from antibiotic resistant bacteria in a triplex assay within 25 min	LOD: 10 DNA copies	56
	Fluorescence microscope	A loop-mediated isothermal amplification (LAMP)-based pathogen nucleic acid detection platform to quantify the amplification rate based on the fluorescent signal	LOD: 10 DNA copies per reaction	57
	Fluorescence microscope	Digital microfluidic Immunocytochemistry in Single Cells (DISC): integrate cell culture, stimulation and immunocytochemistry functions to screen cell signaling response to stimulus at the single-cell level	—	58
	Fluorescence microscope	Digital microfluidic Isolation of Single Cells for Omics (DISCO): integrate DMF with laser cell lysis and intelligence-driven image processing to analyze single-cell genomes and transcriptomes from heterogeneous populations	—	59
		Digital microfluidics-based single-cell RNA sequencing (digital-RNA-seq): enable single cell separation on DMF device, followed by on-chip cell lysis, reverse transcription and cDNA amplification for downstream RNA sequencing	—	19
Chemiluminescence	An integrated photon-counting photomultiplier tube (PMT)	DNA methylation assay: detect DNA methylation level by integrating pyrosequencing process into DMF devices	LOD: 10 pg; can detection DNA methylation level down to 5%	60
	An integrated photon-counting photomultiplier tube (PMT), webcam and laptop	ssDNA-primer-based complex to detect DNA mutations by integrating pyrosequencing process on DMF	Can detect DNA mutation level as low as 5%	61

Table 1 *(continued)*

Detection principle	Instrumentation for integration	Applications	Results (LOD: limit of detection; DR: dynamic range)	Ref.
	PMT, bovine alkaline phosphatase (ALP)	Magnetic bead-based immunoassay to detect insulin and interleukin-6	DR: 1.5–750 pg mL^{-1} (IL-6); 8–1000 pmol L^{-1} (insulin)	62
		Magnetic bead-based immunoassay to detect protein (cardiac troponin I) in whole blood and genomic DNA PCR reaction	Immunoassay detection of TnI protein down to 5 ng mL^{-1} in 8 min; 40-cycle PCR within 12 min	63
	PMT, horseradish peroxidase (HRP) and H_2O_2/luminol	A prototype developed by integrating PMT into a single polar transparent EWOD to analyze the parameters for detection of H_2O_2	LOD: 0.01 mmol L^{-1}	64
	Photodiode; horseradish peroxidase (HRP) and H_2O_2/luminol	Magnetic bead-based immunoassay to separate and detect protein, bacteria and virus	LOD: 30 ng mL^{-1} (HSA); 4×10^4 cfu mL^{-1} (*Bacillus atrophaeus*); 10^6 cfu mL^{-1} (MS2 bacteriophage); 2×10^7 cfu mL^{-1} (*Escherichia coli*)	65
	PMT, horseradish peroxidase (HRP) and H_2O_2/luminol	Magnetic-bead based immunoassay to detect thyroid-stimulating hormone (TSH) under optimal conditions	LOD: 0.15 μIU mL^{-1}	66
		Magnetic bead-based immunoassay to quantitatively detect rubella IgG	DR: 0.15–100 μU mL^{-1} LOD: 0.15 μU mL^{-1}	67
		Magnetic-bead based immunoassay to detect measles and rubella immunoglobulin G (IgG) in field test at Kakuma	LOD: 0.14 mIU mL^{-1} (measles IgG); 0.15 mIU mL^{-1} (rubella IgG)	68
		Magnetic bead-based immunoassay to detect rubella virus (RV) IgG directly from blood	LOD: 1.9 IU mL^{-1}	69
Electro-chemiluminescence	PMT and electrochemiluminescence electrodes	DNA analogue modified magnetic bead-based nucleic acid hybridization assay to detect single nucleotide mismatch microRNAs	LOD: 1.5 femtomoles (miRNA-143)	70
Colorimetry	Bare eyes	Gold/latex bead-based immunoassay to detect goat anti-rabbit antibodies	LOD: 1.0 μg mL^{-1}	71
	LED and photodiode	Enzymatic glucose assay to detect glucose concentration in human physiological fluids	DR: 9–100 mg dL^{-1}	72, 73
	Bare eyes, alkaline phosphate (ALP) conjugated antibody and enzyme	An immunoassay-related enzyme-based colorimetric reaction on a finger-actuated EWOD to detect IgG antibody	—	74
	Smart phone, UV-vis spectrophotometer	Enzymatic assay to detect organophosphorus hydrolase enzyme in paper-based DMF devices fabricated with double-sided electrohydrodynamic jet printing	DR: 10–100 μM (methyl paraoxon and *para*-nitrophenol)	75
	Paper-based analytical device, bare eyes	Integration of a paper-based analytical device and a paper-based DMF to transfer and mix reagents for glucose test	—	76
	Microplate reader, ethidium homodimer-1 stain	Cell-based assay: culture bacteria, algae and yeast on DMF devices (BAY microreactor) to monitor their growth curve	Can grow up to 5 days	77
Surface enhanced Raman scattering (SERS)	Raman detector, Raman reported 4-mercaptobenzoic acid	Immunoassay on a DMF platform to detect avian influenza virus H5N1	LOD: 74 pg mL^{-1}	78
Surface plasmon resonance (SPR)	SPRi prism, LED source and CCD camera	On-chip quantification of DNA hybridization efficiency	Two-fold SPR signal increase within only 8 min of hybridization	79
		Integration of SPRi chip into a DMF platform for on-chip parallel monitoring of bulk medium index changes	—	80
		Integration of SPRi chip containing an array of periodic gold nanostructures into a DMF platform for on-chip quantification of DNA hybridization reaction	LOD: 500 pM	81

Table 1 *(continued)*

Detection principle	Instrumentation for integration	Applications	Results (LOD: limit of detection; DR: dynamic range)	Ref.
Optical micro-resonator	Laser beam, IR camera	Integration of a silicon nanophotonic microring resonator sensor into digital microfluidic device to measure glucose, sodium chloride and ethanol concentration as a proof-of-concept	—	82
	A pump beam, a dichroic beam splitter and spectrometer	Optical cavies used to quantitatively detect molecules (specific binding of streptavidin to a biotinylated) in label-free manner	LOD: 352 ng ml^{-1} (streptavidin)	83
	Halogen lamp based light source, optical fiber patchcords, spectrometer	Integration of a multimode polymer optical waveguide into DMF device to test Au nanoparticles as a proof-of-concept	—	84

substrate of the device after sufficient cleaning. To exploit these advantages, Miller *et al.* immobilized capture antibodies *via* physisorption on the hydrophobic surface of the top ITO substrate.[53] In this work, a droplet containing human IgG moved across the antibody-immobilized spot multiple times to achieve the optimal dynamic binding kinetics instead of the static binding in conventional reactions. The dynamic binding provided a shorter contact time between the antigen in the droplet and the antibody assay, which greatly diminished non-specific absorption. Target antigens were further labeled with fluorescein isothiocyanate (FITC)-tagged secondary detection antibodies by moving the droplet across the immobilization site followed by washing with multiple droplets, and the fluorescence intensity was measured *via* a fluorescence plate reader. The DMF-based immunoassay presented a rapid detection of human IgG within 2.5 hours with high specificity, while maintained the comparable dynamic range and reproducibility as the conventional well plate assays.

Cell-assay. Cell-based assays often measure cell activities (*e.g.*, viability, proliferation and cytotoxicity) in response to various external stimuli at different time intervals. The DMF device is an ideal candidate for these applications due to its automated fluid handling ability that enables reagent replenishing in a programmable manner to regularly feed cells with reduced volume and cross contamination.[49,58,59] To harness these unique advantages of DMF devices for cell-based assays, fluorescence detection has been integrated into these devices to monitor various cell activities. A proof-of-concept study demonstrating the dose–response toxicology screening was reported by Wheeler's group, in which the viability of fluorescently stained T-cells was monitored in response to a series of concentrations of the surfactant (Fig. 3A). This cytotoxicity assay on the DMF platform used $<30\times$ reagents and achieved $\sim 20\times$ sensitivity compared with conventional well-plate assays, highlighting the potential utility of the DMF platform in drug screening. To accommodate different types of cell-based assays with minimal manual steps, further efforts have been focused on improving the automation and versatility of DMF devices. For example, Moazami *et al.* incorporated an automated sample delivery system using a 3D-printed fluidic port to continuously replenish reagents.[52] By incorporating another thermal electric coolers-based closed-loop temperature control interface into the DMF device, this automated DMF platform can perform multiple experiments, including bacterial transformation and enzymatic assays at controlled temperatures. The continuous reagent delivery system improved bacteria transformation efficiency by 7× compared with conventional reagent dispensing methods. In addition, the precise temperature control and reproducible droplet delivery has also improved the sensitivity of fluorescence detection in cellulase-based enzyme assays compared with assays performed in standard DMF devices.

Besides the cell activities mentioned above, the cell invasion assay is another fundamental biological process that has gained significant attention in studying functions of cellular processes.[92] Monitoring cell invasion behavior from one tissue into another can improve the understanding of homeostatic processes such as tissue development and repair as well as pathological processes such as cancer progression. Apart from the aforementioned advantages, the DMF device also supports 3D cell culture by integrating hydrogel microstructures that mimic the extracellular matrix (ECM), as such boosting the key benefits of DMF in cell assay applications. As a result, Li *et al.* developed a digital microfluidic microgel system (CIMMS) with fluorescence detection *via* a 3D high-resolution microscope for a cell invasion assay.[51] This system mimics the invasion of cancerous cells in 3D core–shell structured hydrogels followed by cell extraction for downstream RNA sequencing. Briefly, the core–shell structured microgel was generated in the DMF device by dispensing solution-phase collagen droplets onto hydrophilic spots as the core (Fig. 3B i). After gelation, a solution-phase basement membrane extract (BME) was dispensed to cover the gelled collagen as the encapsulating shells. Immuno-fluorescently stained cells were able to horizontally invade into the hydrogels and allow 2D immunofluorescence imaging in the *x*–*y* plane (Fig. 3B ii). Compared with conventional *z*-dimension cell invasion, this

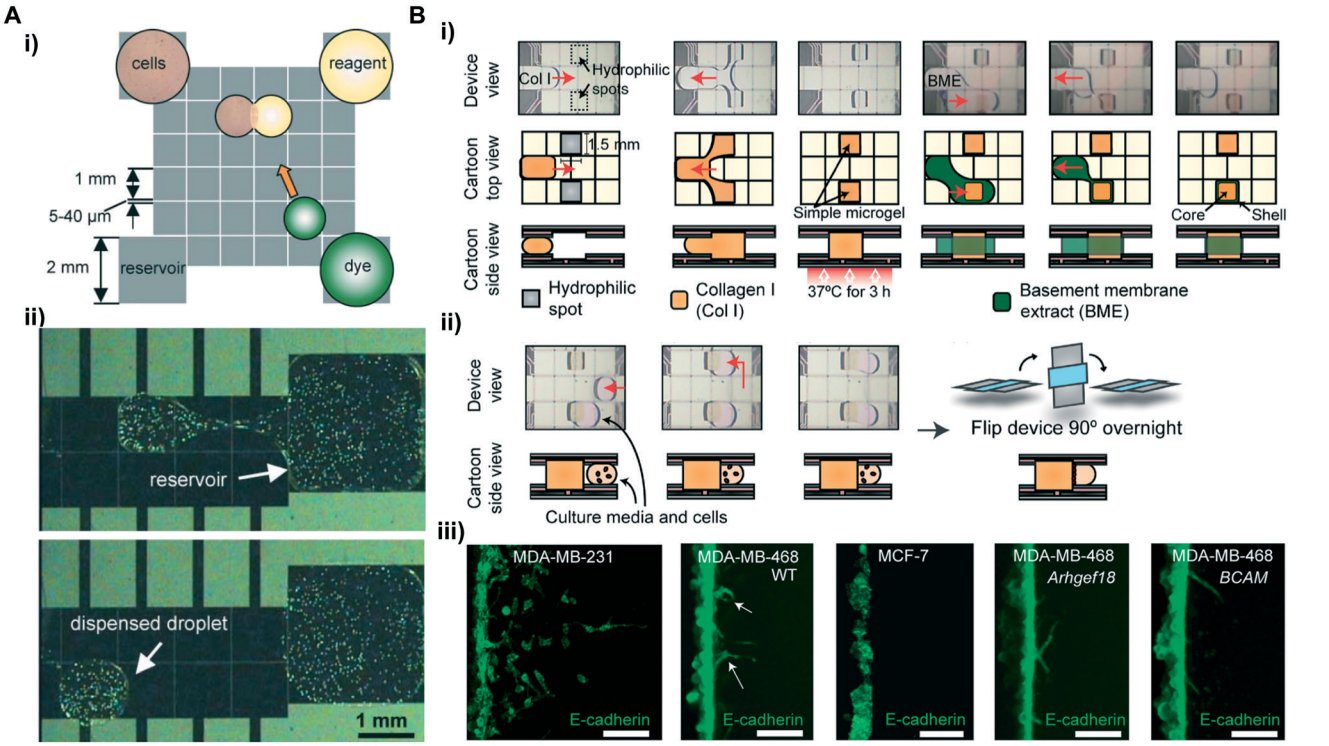

Fig. 3 Cell-assays. (A) Schematic view of a cell assay in a DMF device: i) droplets containing reagent and dye to be incubated with cell droplet; ii) a 150 μL droplet containing ~260 cells is dispensed from a reservoir for fluorescence detection. Printed with permission from ref. 48. Copyright from 2008 Royal Society of Chemistry. (B) i) Photos (top) and cartoons (middle and bottom) describing the formation of 3D core–shell hydrogel in a DMF device; ii) photos (top) and cartoons (bottom) describing cell seeding in a CIMMS assay; iii) comparison of invasion morphologies for breast cancer cell lines by CIMMS. Printed with permission from ref. 51. Copyright from 2020 American Association for the Advancement of Science.

method provided a higher resolution imaging on cell morphology (Fig. 3B iii) for quantitative analysis of the invasion events. Furthermore, the platform enabled a straightforward isolation of cell subpopulations by simply dissecting the microgels (Fig. 3B ii) that contain the invaded cells into thin sections and digesting them to release the cells for downstream RNA sequencing. The combined functionalities made this platform a strong candidate for probing various complex processes that rely on cell invasion (*e.g.*, metastasis, tissue repair) in a comprehensive and efficient manner.

DNA-based application. Besides cells and proteins, DMF devices have also been widely deployed for on-chip nucleic acid amplification and quantification, as they provide low risk of cross contamination in sample preparation. These applications are often centered on detecting specific nucleic acid sequences by amplification. The integration of fluorescence detection into these applications using fluorescent DNA-binding dyes can monitor the amplification process for quality control and further quantify the amplified DNA in real time. For example, Wan *et al.* integrated a fluorescence detection system into a DMF platform to perform loop-mediated isothermal amplification (LAMP) and detect human African trypanosomiasis pathogen *Trypanosoma brucei* DNA.[57] The platform used a low melting temperature (<65 °C) molecular beacon DNA[93] as a probe to recognize the sequence-specific target DNA. Meanwhile, the amplification was fluorescently monitored in real-time with an intercalating dsDNA dye, and the results were read with a microscope mounted above the DMF platform. This real-time monitored amplification presented lower sample consumption (1 μL) with a detection limit of 10 copies per reaction within 40 min, and discriminated non-specific amplification.

3.1.1.2 Chemiluminescence detection. Chemiluminescence detection is based on the chemical reaction between a chemiluminescent substrate and the enzyme label attached to the target molecules. The substrate is often excited by an oxidation reaction forming an intermediate, and when this intermediate returns from the excited state to the ground state, a photon is released and can be detected by a luminescent optical instrument. This method provides high detection sensitivity and a wide linear range of signal response using a relatively simple instrument, and can be used to detect a wide range of targets such as proteins, viruses and chemicals.[65,66,68,69]

The integration of chemiluminescence detection into DMF platforms usually requires photomultiplier tubes (PMTs) to amplify chemiluminescent signals as the submicron volumes of samples and reagents can lead to lowered signals compared with macroscopic volumes. PMTs are able to convert photons into electrons followed by amplifying electrons multiple times,[94]

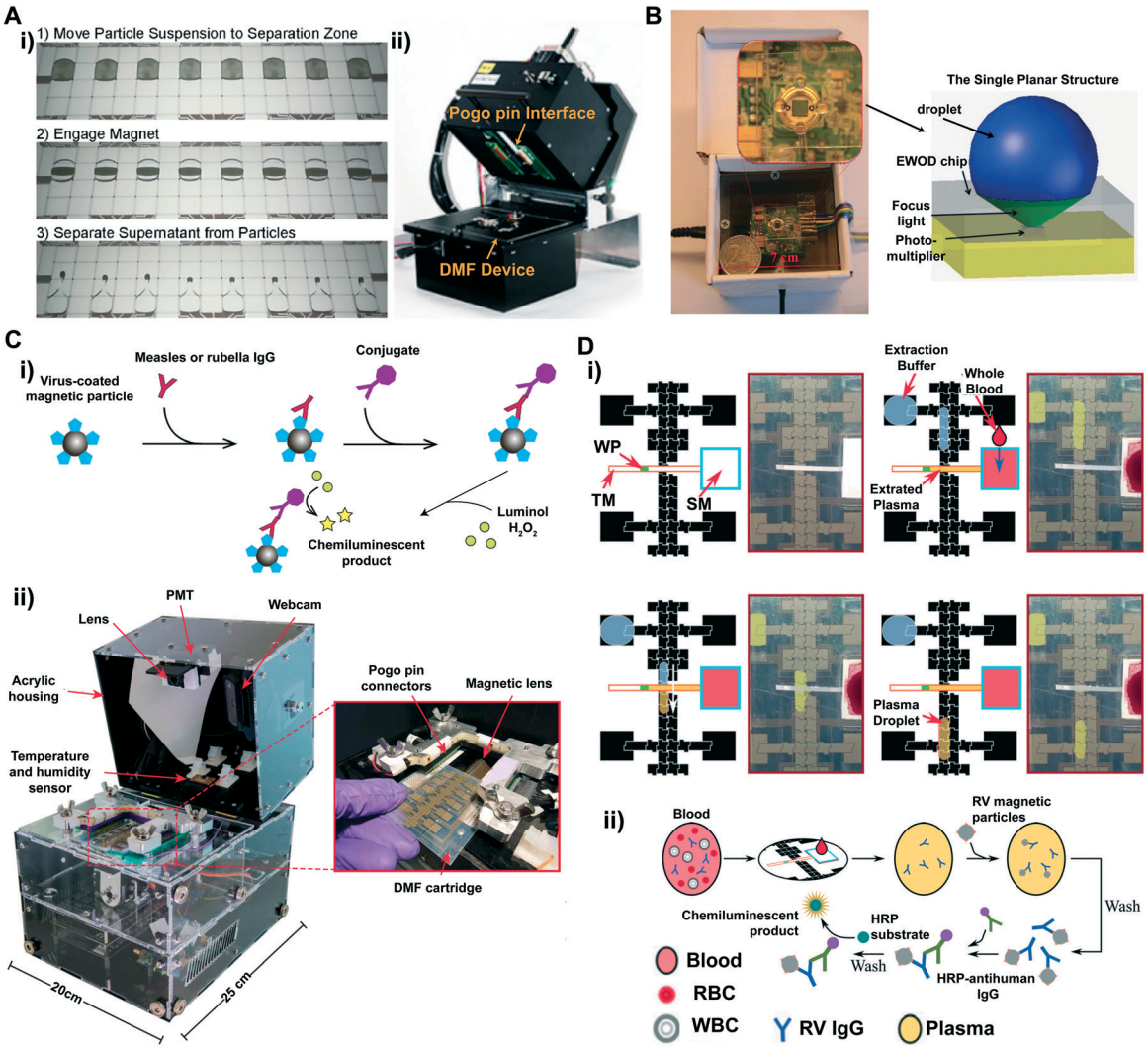

Fig. 4 (A) i) Movie frames depicting the trajectories of the engaging and separation of magnetic particles in a DMF device; ii) picture of magnetic bead-based immunoassays on an integrated DMF platform. Printed with permission from ref. 60. Copyright from 2013 American Chemical Society. (B) A photo of a chemiluminescent detector that contains a single planar DMF chip placed underneath a photomultiplier. Printed with permission from ref. 64. Copyright from 2013 Royal Society of Chemistry; (C) i) schematic demonstration of measles and rubella ELISAs using a H_2O_2–luminol(3-aminophthalhydrazide)–HRP chemiluminescence system. ii) Photos of the integrated measles–rubella (MR) transparent box containing a PMT, a webcam, a temperature and humidity sensor, switching boards and a high-voltage amplifier (underneath the DMF device, not shown in the figure). Zoom-in image demonstrating the insertion of a DMF cartridge into the MR box. Printed with permission from ref. 68. Copyright from 2020 American Association for the Advancement of Science. (D) i) Cartoon diagrams demonstrating the on-chip DMF blood-plasma separation of a finger-stick of blood (WT: wax plug; TM: transport membrane; SM: separation membrane); ii) diagrams depicting the formation of a magnetic particle-based ELISA assay for rubella virus (RV) IgG. Printed with permission from ref. 69. Copyright from 2020 Royal Society of Chemistry.

and thus amplify the signals and reduce the background noises for sensitive detection with a superior signal to noise ratio.[60,95] A straightforward way to use a PMT in the DMF platform is to manually place the light collection window (<1 cm) close above the surface of the device (~5 mm of distance). Used in junction with magnetic bead-based immunoassays, this approach proved effective in quantifying human insulin and interleukin-6 (IL-6) in a glass substrate-based DMF platform (Fig. 4A).[62] The captured proteins were quantified through reading the chemiluminescence intensity of the secondary bovine alkaline phosphatase (ALP) labeled antibodies. The heterogeneous immunoassay on the DMF chip was able to achieve detection within 7 min, presenting dynamic ranges with clinical relevance. To enhance the light collection efficiency into the small window of the PMT, customized gadgets can be used as an interface to focus the emitted beams from the microscale samples. Pamula's group presented an enhanced PMT detection method by attaching a customized lens onto the light collection window of the PMT before placing it above the DMF device built on a printed circuit board (PCB).[63] This integrated platform enabled a magnetic bead-based immunoassay of cardiac troponin I (TnI) protein, and detected as low as 5 ng mL^{-1} TnI in whole blood within 8 min. Further enhanced PMT integration into DMF platforms for chemiluminescence

detection included a motorized PMT as demonstrated by Wheeler's group.[66] In this automated, integrative platform, a pogo-pin electronic interface was built to control droplet movement *via* a computer software interface, and a motor and two optical limit switches were used to control the vertical position of the PMT (a few hundred microns to a few centimeters) and the sensor orifice was automatically protected by a shutter when the PMT was in a disengaged state. Using the same principle, this platform also included a motorized disc that can control the vertical position of a magnetic lens that can focus the magnetic field into a small region in the device for bead separation. In addition, the platform utilized H_2O_2–luminol(3-aminophthalhydrazide)–HRP (horseradish peroxidase) in combination with the enhancer PIP (*p*-Iodophenol) in an immunoassay for enhanced chemiluminescent efficiency.[96–98] As a result, this platform provided an optimized immunoassay by implementing a three-level full factorial design of experiments including varied analyte concentrations, which reduced the incubation time by 2-fold to process ~2-fold sample volume for the screening of hyperthyroidism lower than 0.3 μIU mL^{-1}. The H_2O_2–luminol(3-aminophthalhydrazide)–HRP chemiluminescence system was also adopted by Zeng *et al.*, where they integrated a commercial photomultiplier chemiluminescence detector (~1 square inch) underneath a 2D transparent single planar DMF device in a portable lightproof box (Fig. 4B).[64] The single planar DMF device provided a simplified chip structure and control circuits that can be packed into a palm-sized box. In addition, the ball-shaped droplet on a hydrophobic surface can intrinsically focus the fluorescent beam, thus enhancing the signal intensity. This integrated DMF-based detector measured the concentration of H_2O_2, as a proof of concept. The result demonstrated a sensitive detection of H_2O_2 as low as 0.01 mmol L^{-1}, showing the great potential of the platform as an immune-detector in clinic applications including blood glucose detection.

Electrochemiluminescence (ECL)-based detection can also provide outstanding sensitivity to detect nano-sized biomolecules such as microRNA (miR, ~22 nucleotides).[99] ECL is a novel detection technology in which the emitted light is generated through electron-transfer reactions on the electrode surface,[100] and has several key advantages such as high selectivity, a wide dynamic range and high compatibility with DMF systems.[101] In general, ECL electrodes can be integrated into the top ITO glass substrate, and the ECL signals can be captured using a PMT. By further integrating ECL and the magnetic bead-based assay into a single DMF platform, it is possible to detect miRs with a single nucleotide mismatch at the fM level.[70] In this example, a single stranded DNA probe immobilized on magnetic beads hybridized with miR-143 from MDA-MB-231 and MCF-7 tumor cell lysates; $Ru(Phen)_3^{2+}$ as a luminophore was intercalated into the formed double-stranded helix, and this conjugation along with a co-reactant tripropylamine (TPA) was oxidized under electrical potential, thus emitting photons.[102] The emitted ECL signals can differentiate miRs with nucleotide mismatch and quantify target miR expression levels associated with cancer phenotype.

Overall, the integration of highly reconfigurable DMF platforms and a palm-sized, sensitive chemiluminescent sensing instrument can extend the capability of DMF to detect various nanoscale biomolecules including proteins and DNAs in a rapid and sensitive manner. With the rapid advancement in various technology paradigms such as material engineering and system miniaturization, it becomes feasible to incorporate various features into a single DMF platform. For example, other miniaturized instruments such as the fluorimeter can be integrated alongside the PMT to enable both chemiluminescence and fluorescence detection in a single platform to perform a high-sensitivity immunoassay and to closely monitor DNA amplification in real-time polymerase chain reaction (RT-PCR).[63] As a step toward cost-effective mass production, this type of platform can also be fabricated on flexible substrates (*e.g.*, PET membrane) *via* inkjet printing,[68] broadening its use in resource-limited settings. An example includes measles and rubella screening in the Kakuma refugee camp by forming a magnetic particle-based ELISA assay on the printed DMF device (Fig. 4C i), with 80% on sensitivity and specificity compared with standard ELISA tests. The onsite detections were performed in the portable box (termed measles–rubella box, Fig. 4C ii) containing a PMT and webcam for optical reading and a fully integrated high-voltage amplifier and a signal generator for droplet operation. Further, in a recent effort directed to the processing of finger-stick blood samples in the DMF device for POC diagnosis, additional components such as porous membranes can be integrated for plasma separation (Fig. 4D i), followed by magnetic bead-based ELISA assays for chemiluminescence detection (Fig. 4D ii). These combined strategies enabled the detection of as low as 1.9 IU mL^{-1} rubella virus (RV) IgG from a finger-stick blood,[69] demonstrating great potential for POC diagnosis in remote settings with limited medical resources.

3.1.1.3 Colorimetric detection. The colorimetric technique allows the direct observation of color changes with naked eyes, and therefore attracts great attention in DMF-based assays. For example, Rastogi *et al.* detected IgG and ricin in a DMF-based bioassay that uses the immunorecognition and agglutination of antibody-coated gold/latex particles.[71] In this assay, the gold/latex particles in the droplet were captured under dielectrophoretic (DEP) force and agglutinated at a controlled evaporation rate. As a result, a microscopic readout pattern was formed as an indication of the concentration of antigen as low as 1 μg mL^{-1} present in the droplet. Another popular method in colorimetric detection is the use of paper-based microfluidic analytical devices (μPAD). Compared with conventional substrates such as glass and polymer, μPAD presents practical advantages including low cost and environmental friendliness, suitable for POC applications. Besides, colorimetric detection in μPADs is rapid, user-friendly and can provide visual readout.[103] Despite these advantages, μPADs have limited fluid control capability, and therefore it is challenging to incorporate sample preparation. To fill this gap, Abadian *et al.* presented

a hybrid paper-based microfluidics (HPMF) platform that can handle sample pre-processing and post-processing operations in two units: a DMF device to handle droplets and deliver them to a μPAD for colorimetric detection.[76] Both units were fabricated on a single substrate using a screen printing method, and the exit of the DMF unit was aligned with the entrance of the μPAD. This hybrid platform enabled the detection of as low as 100 mg dL^{-1} glucose in 30 min and provided a promising outlook for integrating different microfluidic paradigms with unique strength into a single platform that is sensitive while being cost-effective and straightforward for biomarker detection.

As colorimetric detection is simply based on color intensity, a limitation is the lack of standard for quantitative analysis, and the reading is rather subjective and can be affected by factors such as the ambient lighting condition. To improve the detection accuracy, efforts have been focused on developing a quantitative method to analyze the results. Absorbance measurement, as one of the most commonly deployed quantitative colorimetric analysis methods, can quantify the absorbance intensity of the monochromatic radiation by the analytes. This measurement usually requires a photometer comprising a light source and a detector (*e.g.*, photodiode) assembled between analytes. Light-emitting diodes (LEDs) are a popular type of light source characterized by being low-cost (<$1), portable and robust (up to 10^4 h lifetime) that are suitable for miniaturized analytical devices for colorimetric-based POC detection. In devices with transparent substrates, this setup can be easily integrated. Srinivasan *et al.* reported a colorimetric enzyme assay in a DMF device to measure glucose concentration ranging from 25–300 mg dL^{-1} within 1 min. The DMF device was directly sandwiched between a green LED to illuminate the sample and a photodiode to convert the optical signal into an electrical current as the readout.[72,73] The absorbance rate of the samples was measured over time, as the colorimetric enzyme-kinetic method was based on Trinder's reaction. In devices that are built on non-transparent substrates (*e.g.*, PCB substrates), however, apertures are often needed to accommodate the integration. For example, Gu *et al.* integrated absorbance measurement into a palm-sized, reusable DMF system constructed on a PCB board.[104] This platform embedded an aperture on the opaque PCB board, creating a light path between the LED and the photodiode for optical sensing. Creating apertures on substrates can require alternative device fabrication methods, due to the technical challenge of creating apertures on the sensing area without compromising the quality of the surrounding thin dielectric layer that is vital to the central functionality of the device. Therefore, instead of spin coating, this work used an electrostatic film-posting method to assemble a poly-(tetrafluoroethylene) (PTFE) film (10 μm thickness) as a hydrophobic dielectric layer on the PBC substrate. The platform showed high sensitivity of quantitative detection of nitrite with good linearity (R^2 = 0.9974) with a limit of detection of 5 μg L^{-1}, which is lower than the nitrite cut-off level in drinking water (13 μg L^{-1}) according to the World Health Organization (WHO). Two or more LEDs can be integrated in this manner, and other methods (*e.g.*, gold nanoparticles) can be incorporated to enable the sensitive, parallel detection of several small molecules.[105] However, the narrow emission spectrum (400–700 nm) of LEDs can limit multiplexed detection without compromising accuracy. Potential solutions include the use of UV-LEDs and IR-LEDs that exhibit wide spectral emission (250 nm to 4.6 μm).

The use of photometers in DMF devices needs a transparent optical path for the colorimetric assay, which either limits the selection of actuation electrodes to be transparent or requires more complex fabrication to create a light path. As an alternative, measuring the reflection of incident light on the substrates can circumvent the challenge. This detection model usually relies on capturing "digital images" with cameras and converting the captured photons into electrical signals through the photodiode for color intensity analysis. Smartphone-based colorimetric detection, in recent years, has provided an outstanding performance for spectroscopy applications due to many improved features such as a high-resolution camera and various image processing software programs. These cameras usually have complementary metal-oxide semiconductor (CMOS) photodiode chips that can readily convert captured photons into electrical signals, thus reflecting the color intensity. Meanwhile, compared with bulky optical setups, imaging on personal electronics can be an attractive alternative for data collection, processing, storage and transfer for medical assessment. Jafry *et al.* adopted a smartphone-based colorimetric detection platform to a paper-based digital microfluidic (PBDMF) device, and quantified methyl paraoxon (MPO) levels based on an enzymatic reaction.[75] The resulting changes in color intensity were monitored with a smartphone and the data was processed using the ColorAssistant app. Further digital graphic analysis used a Bayer filter to assign the captured figure to different color spaces – RGB (red, green and blue) that mimics human vision. The established RGB color matrices represent the intensity of each component, which can further reflect the measured analyte concentration. Kanitthamniyom *et al.* utilized this colorimetric analysis method to analyze the color changes resulting from the reaction of carbapenemase-producing *Enterobacteriaceae* (CPE) hydrolyzing carbapenem antibiotics, to identify CPE on a magnetic DMF device.[106] The resulting color shifts were objectively mapped into a chromaticity diagram CIE color space[107] *via* a smartphone app, which ruled out subjectivity-induced variations. In this manner, the antibiotic resistance of the target bacteria was identified with comparable sensitivity and specificity to the Carba NP test (a biochemical test of carbapenemase production in a Gram-negative bacterium) with reduced sample consumption (up to 90%). With the rapidly evolving advancement in personal electronics, computing algorithm and system miniaturization, we anticipate that smartphones can be empowered to bring POC testing to bedsides and homes, as well as remote or low-resource settings.

3.1.1.4 Surface Enhanced Raman Scattering. Surface Enhanced Raman Scattering (SERS) is a sensing technique that describes the enhanced Raman scattering of molecules that are absorbed onto metal nanostructures (*e.g.*, gold nanoparticles and silver nanoparticles) when objects are exposed to a laser beam. In general, the enhancement is attributed to the coupling between the incident light and the localized surface plasmon resonances (LSPR) on these nanostructures,[108] resulting in the enhanced electromagnetic field (termed electromagnetic enhancement). This enhanced electromagnetic field further boosts Raman scattering intensity when molecules are near the nanostructures. Another theory describes the enhancement mechanism as a charge-transfer complex formation when the molecules bind to the surface of the nanostructures.[109] Though the main mechanism of the enhancement is still under debate,[110] SERS provides highly sensitive detection due to the enhanced Raman scattering signals, and is especially suitable for detecting low-abundance molecules in complex media.[111,112] Additionally, due to the narrow peak of Raman scattering compared with the fluorescent/luminescent emission band, SERS is more advantageous in multiplex detection.[113] Using this detection strategy, Wang *et al.* quantified avian influenza virus H5N1 in human serum in an automated DMF device.[78] In this device, core(Au)–shell(Ag) nanostructure was constructed as a SERS tag and this nanostructure was embedded with 4-mercaptobenzoic acid as a Raman reporter. The SERS tag was then conjugated with detection antibodies to label the target H5N1 virus captured by a magnetic bead-based immunoassay. SERS spectra were obtained from a portable Raman spectrometer, and the scattered beam was directed into a charge-coupled device (CCD) detector, and the concentration of H5N1 was quantified based on the intensity of Raman scattering. This automated device detected as low as 74 pg mL^{-1} H5N1 in ~30 mL human serum within 1 hour, presenting excellent sensitivity for screening viral infections.

3.1.2 Label-free optical techniques. Although the previously mentioned methods provide highly sensitive, accurate and selective detection of biomolecules, the use of labels can complicate the entire process, rely on skilled technicians and lag sample-to-answer time. Therefore, recent effort toward label-free operation offers alluring prospects for the rapid and simple detection of biomolecules with reduced use of reagents in minimally trained hands. Major label-free detection mechanisms that have been integrated into DMF devices include surface plasmon resonance (SPR) sensors and micro-resonators.

SPR is a phenomenon where the electrons in the metal surface layer are excited by photons of incident light at a certain angle of incidence, and then propagate parallel to the metal surface. Based on this principle, SPR provides a quantitative detection of molecules in a label-free and real-time manner. With a constant wavelength of the light and the metal, the angle that triggers SPR is dependent on the refractive index of the material near the metal surface. Consequently, a small shift in the reflective index (*e.g.*, biomolecule attachment) of the sensing medium will hinder the occurrence of SPR, and the shift is correlated to the mass of molecules on the surface.[45] Therefore, SPR-based detection can provide highly sensitive recognition of nanoscale molecules such as DNA. Given the intrinsic parallel processing ability of DMF platforms, integrating SPR-sensors into these platforms can greatly boost the detection efficiency.[114] As a result, Tabrizian's group integrated a series of surface plasmon resonance imaging (SPR-i) interfaces into a DMF device for label-free and multiplexed DNA detection in real-time.[79–81] In essence, the platform was composed of an Au-coated SPR-i chip as the top plate and Au actuation electrodes on the bottom plate (Fig. 5A i) and ii)).[79,80] The bare SPR-i detection electrodes were patterned on the hydrophobic Teflon layer using lift-off technology. When a

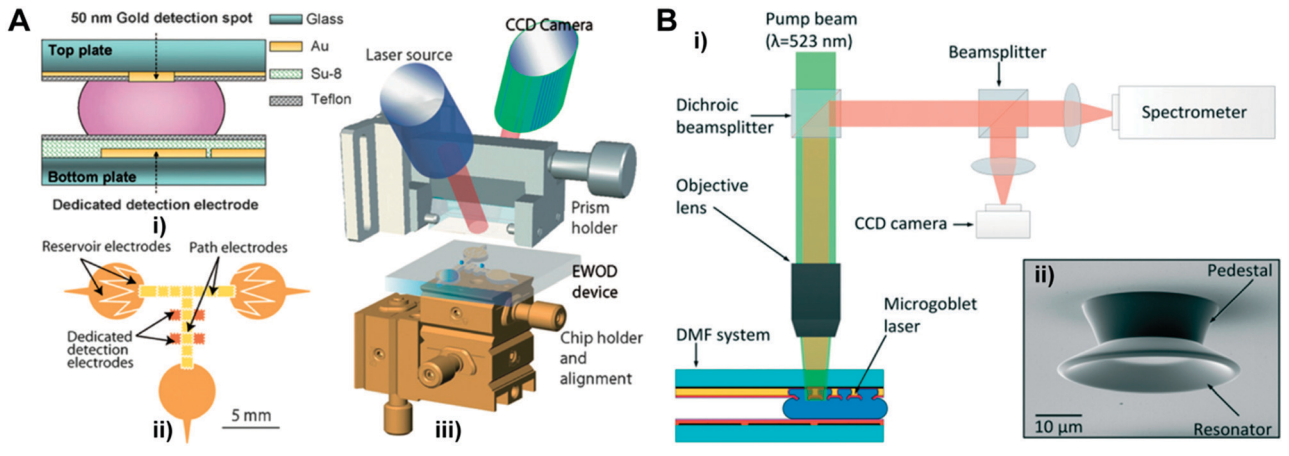

Fig. 5 (A) i) Cross-section diagram of a DMF chip coupled with surface plasmon resonance imaging (SPR-i). ii) Layout of the bottom plate that contains reservoir electrodes, path electrodes and detection electrodes. iii) Diagram of the SPR-i coupled DMF platform. Printed with permission from ref. 80. Copyright from 2009 Royal Society of Chemistry; (B) i) an integrated DMF system containing pumping and read-out of a micro-goblet laser array as biosensors. ii) Scanning electron micrograph (SEM) of a single micro-goblet laser. Printed with permission from ref. 83. Copyright from 2017 Royal Society of Chemistry.

droplet of the DNA immobilization reagent was moved to the detection electrodes, DNA probes were efficiently immobilized on the electrodes by forming the Au–sulfur covalent linkages between the thiolate DNA probes and Au electrodes under the applied electric field. The SPR signals were measured by mounting the DMF device onto the chip alignment stage and adjusting the position of the device to couple it with the SPRi prism (Fig. 5A iii)). The SPR-i signal was enhanced by the nanostructured periodic gold nanoposts at the detect sites, achieving a 200% increment on the SPR-i signal at a limit of detection of 500 pM (90 attomoles).[81] Despite the superior sensitivity, the detection largely relies on advanced, specific optical systems (*e.g.*, laser, CCD camera) in laboratory settings. Meanwhile, precise chip alignment is required to couple the microscale detection electrodes with the optic components such as the SPR prism. To extend the use of highly sensitive detection platforms as such to POC applications, further system integration and miniaturization (*e.g.*, portable SPR systems[115,116]) are necessary to ultimately bring the rapid, quality care from lab benches to bedsides.

More recently, silicon photonics-based optical sensing systems are becoming appealing due to their ability of large-scale integration and mass production. Optical micro-resonators, as one of the integrated silicon photonic structures, are promising in POC applications due to their superior detection sensitivity at the molecular level. In optical micro-resonators, microstructures (micro-resonator) are integrated to confine light to a certain trajectory for multiple passes *via* reflection. This confined resonant mode amplifies the signal from the light beams and therefore enhances molecular sensing. The molecules present on the micro-resonator surface can lead to changes in the refractive index (RI) in a similar way to those in SPR-based sensors, but in micro-resonators, these changes can further lead to shifts in resonance wavelength.[82,117,118] Based on this principle, Lerma Arce *et al.* incorporated a silicon nanophotonic micro-ring resonator into a DMF to achieve label-free detection in real-time.[82] In this platform, a silicon-on-insulator (SOI) chip was used as the sensing component on the top substrate of the DMF device owing to its high refractive index contrast, which eliminated the need for bulky instruments such as high power lasers and spectrometers, while the droplet was handled on the bottom plate. The SOI chip contained an array of micro-ring resonators consisting of waveguides and directional couplers. A tunable laser beam was used to excite the input waveguides through the input grating couplers, and the output signals from ring resonators were coupled to free space through an output grating coupler, and the signal was then imaged on an infrared (IR) camera. In this platform, analytes in the bulk liquid (*e.g.*, sodium chloride, glucose, ethanol) were detected with comparable sensitivity (~77 nm RIU^{-1}) as typical microchannel-based systems (78 nm RIU^{-1}).[119] However, detection of analytes in bulk solution usually lacks specificity, and improvements require future efforts on implementing immunoassays on micro-resonator surfaces to recognize target molecules, allowing label-free and specific detection.

As conventional micro-resonators usually confine the light between two parallel microscale mirrors, this poses challenges in mirror alignment during device fabrication. The whispering gallery mode (WGM) resonator circumvents this challenge by utilizing azimuthally symmetric geometry structures such as spheres and toroids, to circulate light beams through multiple internal reflections, and therefore can provide sensitive detection of biomolecules down to the single molecule level.[120,121] The detailed WGM enhancement mechanism is introduced elsewhere.[122,123] A WGM resonator-based sensing system is typically label-free, and the detection is based on the shifts in resonance wavelength caused by changes in the surrounding media or the refractive index of resonance due to the binding of molecules. Wondimu *et al.* first integrated a WGM resonator into a DMF platform and detected molecules by measuring the binding of streptavidin to the biotinylated sensor surface.[83] In this detection platform, micro-goblet laser arrays were fabricated with laser dye doped poly(methyl methacrylate) (PMMA) on the top layer of the DMF device, and the array was excited with the pump beam (Fig. 5B). The laser dye doped in resonators served as an optically pumped laser and enabled the free-space excitation and readout of resonance wavelengths. This detection scheme does not require complex structured fiber-coupled elements such as conventional taper fibers, and thus is well suited for large-scale sensor arrays.[124,125] The refractive index sensitivity of this integrated sensor was demonstrated to be 28.11 nm RIU^{-1}, which was ~3× lower than previously mentioned micro-ring resonators (~77 nm RIU^{-1}).[82] In addition, the platform showed a quantitative detection of streptavidin with a sensitivity of 3.83 pm μg^{-1} ml, indicating its potential to detect various clinically relevant biomolecules with high sensitivity.

Overall, label-based optical detection methods can often be integrated into DMF devices with minimal device modification. Among these, the fluorescence technique is the most widely deployed due to its high sensitivity and selectivity in various assays. However, it requires light sources to provide excitation wavelength and detect the emitted wavelength, and a key challenge is the spectral overlap in multiplex detection. Chemiluminescence technology, as a method with a higher sensitivity (10^{-18} to 10^{-15} mol L^{-1}),[126] eliminates the need for external light sources. Detection systems such as commercial PMTs can be easily coupled with DMF platforms, therefore chemiluminescence detection is a promising detection strategy. However, the common limitation of the fluorescence and chemiluminescence technology is the relatively wide emission band, which makes it difficult for multiplex detection of a large panel of analytes. Colorimetric detection, as an alternative, uses low-cost LEDs as light sources and portable photometers or smartphones as detectors, and thus can be potentially integrated with personal electronics and used as self-administrated POC tests. However, the sensitivity is often lower than

fluorescence/chemiluminescence detection. Besides, one general issue for label-based optical technologies is that the intensity of the optical signals largely depends on the sample volume, presenting a challenge when the technologies are used to detect targets in submicron droplets in DMF devices.[127] Label-free technologies such as SPR, on the other hand, often measure the shifts in refractive index or wavelength upon the molecule interaction. These methods provide excellent sensitivity and are well-suited for multiplex detection. However, the major challenge of integrating these methods into DMF devices lies in the complexity of device fabrication, the precise alignment of highly specialized optical instruments and often the requirement of trained personnel.

3.2 Electrical techniques

Electrical biosensors have gained significant attention in POC diagnostics because they are often robust, easy to miniaturize and cost-effective. One of the key components in electrical biosensors is the transducer that converts biorecognition events into electrical signals such as current and conductance. Thus, based on the mechanisms in which the electrical signals are converted and measured, electrical biosensors are often categorized into an electrochemical biosensor (measures the potential or charge accumulation), an impedance biosensor (measures the electrical impedance of an interface) and a field-effect transistor biosensor (measures current/potential across a semiconductor).

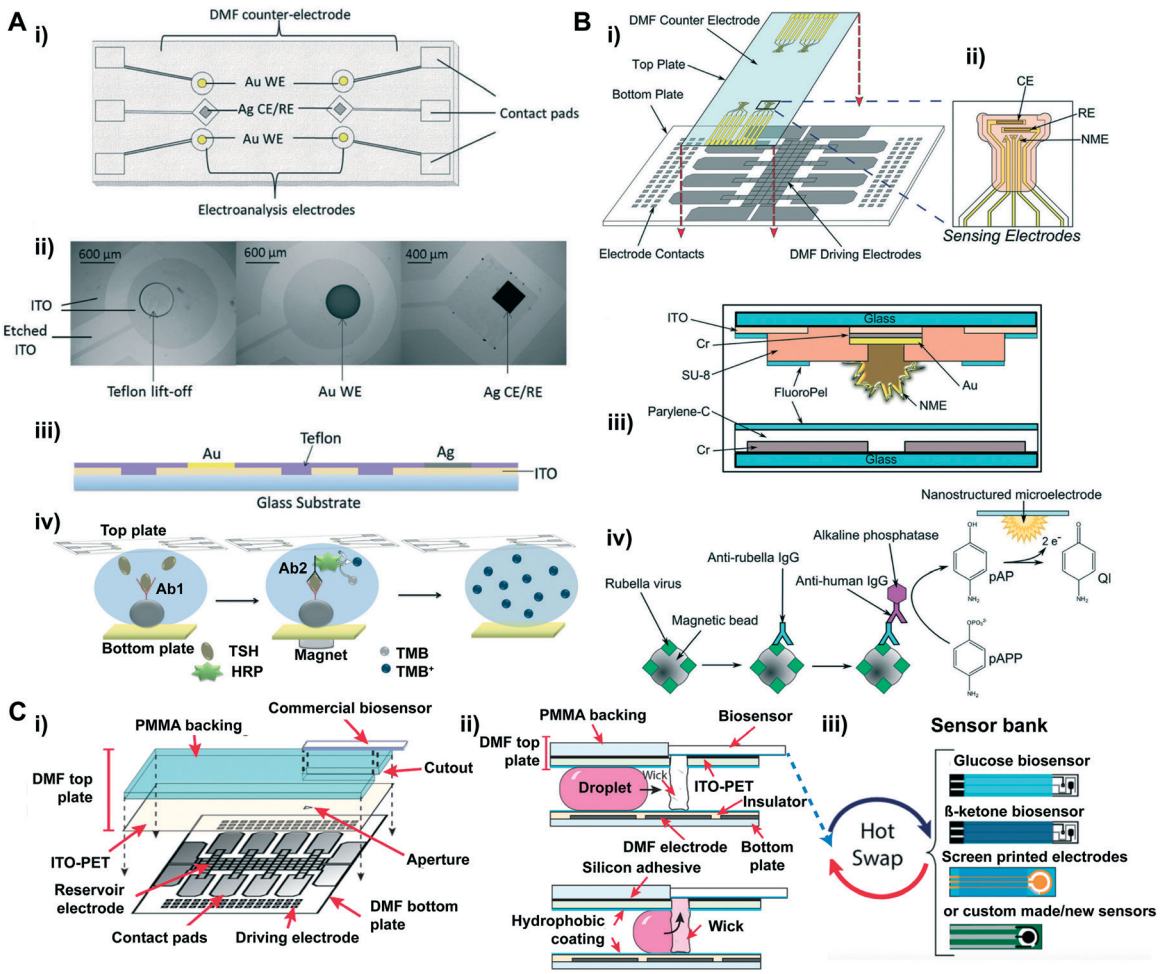

Fig. 6 (A) Electroanalysis integrated DMF system: i) top view; ii) optical microscope; iii) side-view schematic of the top plate configured with electrochemical electrodes. Six electroanalysis electrodes containing four gold working electrodes (WE), and two silver counter electrodes/reference electrodes (CE/RE). Electroanalysis electrodes were fabricated by electroplating on Teflon lift-off spots on the ITO top plate. iv) Schematic illustration of DMF electro-immunoassay. Printed with permission from ref. 133. Copyright from 2014 Royal Society of Chemistry. (B) Diagram of nanostructured microelectrodes (NMEs) integrated into a DMF device. i) A computer-rendered diagram showing the assembly of a DMF device containing four sensing electrodes. ii) Zoom-in diagram of sensing electrodes: a NME as WE, and two CE and RE. iii) Cross-section diagram of the NME-integrated DMF chip. iv) Schematic illustration of DMF electro-immunoassay. Printed with permission from ref. 137. Copyright from 2014 Royal Society of Chemistry; (C) cartoon diagrams of "Plug-n-play" DMF (PnP-DMF). i) Schematic diagram showing the assembly of PnP-DMF. ii) Cross-section of the PnP-DMF device demonstrating the movement of a droplet to the absorbent wicks and its further delivery to the electrochemical cells. iii) Illustration of "hot swap" of different types of biosensors on the DMF top plate. Printed with permission from ref. 141. Copyright from 2019 American Chemical Society.

3.2.1 Electrochemical sensors. Electrochemical sensing is a common detection method that measures the electron transfer associated with the oxidation/reduction rate in chemical reactions that occur on electrode surfaces.[128,129] The sensor generally consists of three electrodes: working electrode (WE, where chemical reactions take place), counter electrode (CE, which carries the current with the WE) and reference electrode (RE, which measures the potential of the WE). Based on the types of signals to be measured, electrochemical sensors are mainly categorized into three types: current (voltammetry/amperometry), potential (potentiometry) and impedance (electrochemical impedance spectroscopy). The principle and advantages of each category have been summarized in detail in the literature.[128,130] Here, we will mainly focus on the integration of electrochemical sensors into the DMF platform for the on-chip detection of biomolecules.

A main challenge in integrating the electrochemical sensor into DMF platforms is the fabrication of hydrophilic, bare sensing electrodes that are precisely situated within the microscale actuation electrodes. A straightforward way is to photolithographically pattern the sensing electrodes within actuation electrodes that are insulated with photoresists (*e.g.*, SU-8).[131,132] Platforms built in this manner can quantify chemicals and drugs, for example, acetaminophen drug with 76 μM detection limit, presenting comparable detection performance with a commercial screen-printed electrode.[95] However, the fabrication is challenging and time-consuming because multiple layers including metal and thin films need to be precisely patterned on the same substrate in a stepwise manner. Meanwhile, the hydrophilic area within the hydrophobic actuation electrodes can impede the electrowetting-based droplet handling. As an alternative, patterning the sensing electrodes on the top ITO substrate can simplify the fabrication procedure and maintain smooth droplet handling (Fig. 6A i–iii).[133] DMF devices fabricated in this manner enabled magnetic bead-based electroanalytical immunoassays for amperometrically quantifying biomarkers such as thyroid stimulating hormone (TSH) with a limit detection of 2.4 μIU mL^{-1} (Fig. 6A iv)). DMF platforms as such can also be used for monitoring cell growth, differentiation and drug uptake *in vitro*. Wheeler's group analyzed dopamine uptake by dopaminergic neurons in an integrated DMF system for neurological disorder diagnosis.[134,135] In their study, neuronal cells were cultured and incubated with dopamine droplets in the DMF device, and the sample was then shuttled to the two-electrode electrochemical sensor patterned on the ITO ground electrode for in-line electrochemical measurements.[134] As low as 30 nM dopamine uptake was determined within 10 min. Further improvement was made on this platform to streamline cell culture and electrochemical characterization on-chip to determine the dopamine uptake in a time-resolved manner.[135] In this platform, automated cell medium exchange during the culture procedure minimizes manual steps and contamination, and the in-line cell assay characterization provides dynamic analysis in real-time, moving closer toward the reality of lab-on-a-chip.

In electrochemical sensors, the number of probes that the sensing electrode can accommodate is a major determinant of the sensor's detection limit. Therefore, recent efforts have been directed towards enhancing the detection sensitivity by increasing the surface area of the electrodes to accommodate more binding sites for molecular probes, thus capturing more targets which eventually lead to higher electron transfer rates.[136] An effective way of increasing the probe binding sites on the electrode is to turn the surface of the electrode into a corrugated format. Wheeler's group, for example, integrated 3D electrochemical sensing electrodes, termed nanostructured microelectrodes (NMEs), into a DMF platform (Fig. 6B i and ii).[137] The NMEs were fabricated by electrodeposition of gold onto working electrodes (WEs) pre-patterned on the top plate of the device (Fig. 6b iii)), and these electrodes presented >600× peak signal magnitude in response to the oxidation process compared with planar electrodes. This device was able to detect as low as 0.07 IU mL^{-1} rubella virus (RV) (Fig. 6b iv), which is >100× lower than the cut-off for rubella immunity defined by the World Health Organization.

In the previously mentioned methods, electrochemical sensing electrodes are normally patterned on the glass substrate of DMF devices *via* conventional photolithography and ion beam deposition. However, these methods rely on relatively expensive and complex fabrication procedures which limit mass production of the devices. Current commercial laboratories usually use screen-printing technology (SPE) to mass produce disposable electrochemical biosensors for POC applications, as it provides cost-effective, simple and highly producible means to fabricate electrodes in bulk quantities.[138] This technology also holds a high degree of flexibility in the selection of electrode materials, such as silver and carbon ink, and can be further implemented for versatile applications.[139,140] This offers a selection of commercial sensors to be readily used in junction with other technologies such as DMF platforms to streamline sample preparation and detection processes in a single device. Leveraging from commercial electrochemical sensors requires a way to interface the sensors with DMF devices in a user-friendly manner, Wheeler's group developed a novel DMF-based electrochemical detection platform compatible with external sensing chips (Fig. 7C i), which allows for commercial electrochemical sensors to be plugged in, termed as "Plug-n-Play (PnP)" (Fig. 7C iii).[141] Briefly, in this device, the ITO-coated PET substrate was backed on a PMMA plate with a cut-out for interfacing commercial sensors, and droplets were delivered through an aperture on the top plate (Fig. 7C ii). This platform enabled a "hot-swap" detection of multiple analytes (glucose, β-ketone and lactate) from both the supernatant and precipitate of single sample-aliquots during an ongoing experiment by simply replacing the commercial sensor in action, including commercial screen-printed electrode cells and customized paper-based

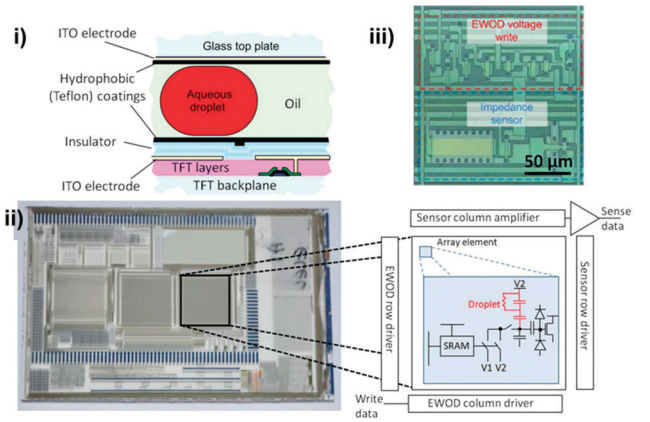

Fig. 7 Active matrix electrowetting on dielectric (AM-EWOD) device containing a 64 × 64 thin film transistor (TFT) array. i) Cross-section of the array: top layer contained ITO as the ground electrode and a hydrophobic layer; bottom layer comprised ITO electrodes patterned on the TFT layer as actuation electrodes and a TFT backplane was fabricated at the bottommost layer to further connect with a PBC board. ii) Photo image of an AM-EWOD chip containing 3 arrays, and the zoom-in diagram of the simplified TFT electronic circuit. iii) A picture of a single array element circuit containing an EWOD droplet operation region and an impedance sensing region. Printed with permission from ref. 143. Copyright from 2012 Royal Society of Chemistry.

sensors. This DMF platform provided high flexibility on accommodating disposable commercial electrochemical sensors, which offers alluring prospect for multipurpose diagnosis in POC testing.

3.2.2 Impedance sensor. In a DMF device, a capacitor is formed when a droplet resides between two parallel planar electrodes (actuation electrode on the bottom and ITO ground electrode on the top). The volume and location of the droplet can then be tracked in real-time by measuring the capacitance changes of the droplet compared with a reference electrode.[142] Therefore, impedance sensors have been used in DMF systems to obtain real-time feedback on droplet location and volume.[142–145] Morgan's group reported the first large active matrix electrowetting on dielectric (AM-EWOD) device that contains 4096 independently programmable electrodes. The platform was controlled by a thin film transistor (TFT) array, and each element was integrated with a circuit to measure the electrical impedance of the droplets (Fig. 7), making it possible to simultaneously and accurately estimate the droplets' position and volume.[143] This platform is increasingly complex in design and fabrication, however, it extends the possibility to integrate other components into the TFT arrays in a highly compact manner. As a further effort, a metal thermistor-based temperature sensor was incorporated into the TFT substrate to systematically control the performance of isothermal reaction recombinase polymerase amplification (RPA) on-chip,[54,56] and a customized optical setup was then built[55] into the platform to quantify the antimicrobial resistance gene. In this platform, DNA containing $bla_{CTX\text{-}M\text{-}15}$ extracted from *E. coli* was fluorescently detected with single copy resolution within 15 min. In a platform like this, processes from sample and reagent preparation to detection can be integrated into a single device, and the device can be reconfigured to simultaneously perform multiple processes on-demand, making it a universal tool for screening various diseases that require different assays and protocols.

In DMF devices, changes in droplet composition can also lead to changes in the capacitance of the droplet between two planar electrodes, and thus be detected by the impedance sensors on DMF. This can be achieved by isolating the sensing regions from the actuation electrodes. For example, Lederer *et al.* constructed a pair of impedance measurement electrodes on a glass slide and mounted them on a single-plate DMF device, and the sensing electrodes were aligned to be situated between two adjacent actuation electrodes to achieve droplet actuation and impedance sensing at the same time.[146] This platform can differentiate NaCl solution with different concentrations (0–0.9%). Blume *et al.* developed a similar integrative platform[147] which leveraged an interdigitated electrode to achieve higher sensitivity on the detection of protein solutions. Although integrating impedance sensors on an insulated actuation electrode is relatively straightforward, the detection sensitivity can be compromised as the dielectric layer largely impedes the conductivity. Moreover, the dielectric and hydrophobic layers can hinder the recognition of target molecules on the sensing electrode, thus limiting the applications to non-specific detection in bulk solutions. Instead, bare electrodes can enhance the sensitivity and specificity in the integrated platforms, although patterning these bare electrodes precisely situated with dielectrics/hydrophobics-coated actuation electrodes can be more complex and challenging as discussed in the Electrochemical sensors section.

However, manipulating droplets on the hydrophilic biosensor surfaces within arrays of electrodes coated with hydrophobic coating can be challenging. As a droplet moves across a sensing electrode, a residual droplet will be trapped due to the reduced surface contact angle of the sensing electrode compared with the surrounding hydrophobic actuation electrodes, hindering its further movement to the adjacent electrode. It would be ideal to adopt electrodes with geometries that offer maximal target binding sites and minimal interference with droplet handling. Samiei *et al.* thoroughly analyzed the influence of sensing electrodes with regard to their hydrophilicity and geometry to identify the optimal electrode geometry for the detection of molecules in the DMF platform.[148] To obtain the largest sensing area without inhibiting droplet removal after sensing, a set of interdigitated electrodes (IDE) with a high aspect ratio was patterned on the top substrate and aligned with the center of the actuation electrodes underneath. The optimal configuration of sensing electrodes was able to quantify cryptosporidium down to 15 cells per μL based on the capacitive changes. Compared with conventional V-notch square electrodes, fractal electrodes can carry a uniform and

intense electric field. Therefore, another DMF platform used novel two-terminal fractal electrodes as both actuation and sensing electrodes which enhanced droplet transport.[149] On these fractal electrodes, 0.5 mg L^{-1} C-reactive protein (CRP) was detected within 3 min, a cut-off set by the American Heart Association (AHA).

In addition to the static measurement of target molecules, impedance sensing is an attractive method for dynamic monitoring in DMF platforms as the attachment of a target on the electrode can alter the impedance value in real-time. Using this method, Wheeler's group monitored cell growth over days and time-longitudinally quantified cell density at a limit of detection of ~20–25 cells per mm^2 in a DMF device.[150] Compared with a conventional electric cell substrate impedance sensor (ECIS), this system held ~1000× reduction in reagent consumption. Moreover, the intrinsic droplet handling ability of DMF provided an automated media exchange during the cell culture, presenting great potential for monitoring the dynamics of cell growth and therapeutic effects.

3.2.3 Field effect transistor (FET) biosensor. The FET biosensor (Bio-FET) is another promising electrical biosensor for POC diagnosis given its advantages of label-free, sensitive and rapid biomolecule detection.[151] The FET consists of three semiconductor components: source, drain and gate electrodes, in which electrical charges start from the source electrode, pass through the gate electrode and end at the drain electrode. The flow of the electrical current can be modulated by applying voltage to the gate electrode, as this alters the conductivity between the drain and source electrodes. In a bio-FET, a biological recognition element is immobilized on the gate electrode for molecule recognition, and the binding of charged biomolecules can lead to the change of the charge distribution, resulting in conductance change on the gate electrode.[152,153] Since the FET is considered as a transducer in the biosensor, it presents real-time responses to the binding events. Therefore, the integration of a DMF device and FET sensor offers great flexibility and rapid detection in POC applications. In a study reported by Choi *et al.*, a FET biosensor was integrated into a single-plate DMF device built on a silicon substrate to detect avian influenza antibody.[154] In this device, the FET electrodes were fabricated at the center of the actuation electrodes, and a thin layer of silicon dioxide was deposited on the FETs to isolate the sensing electrodes from the actuation electrodes (Fig. 8i). Molecule binding occurred in the "underlap region" between the gate and the drain electrodes (Fig. 8 iii and iv). Avian influenza virus linked with the silica-binding proteins (SBP-Ala antigen) was immobilized on the surface of the "underlap region". In this single-plate device, droplet manipulation was achieved by "pre-charging" the droplet on the pre-charging electrodes (Fig. 8ii), followed by applying opposite polarity voltage to the adjacent electrode to move the droplet *via* electrostatic attraction force.[155] As droplets containing target antibody moved to the FET sensing electrodes and interacted with the SBP-Ala antigen functionalized surface, the drain current was reduced, indicating the presence of the avian

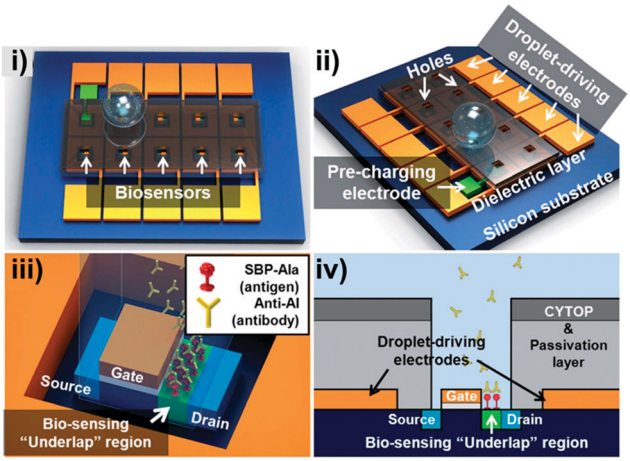

Fig. 8 Schematic of the FET-based DMF platform for the detection of avian influenza antibodies. i) Top- and ii) side-views of the integrated platform. Inter-layer dielectric (ILD) silicon dioxide as a dielectric layer was deposited on the actuation electrodes with holes in the center for droplet contact. iii) Magnified image of the underlap FET biosensor demonstrating the recognition of antibodies and SBP-Ala antigens immobilized on the surface. iv) A cross-sectional view of the underlap FET biosensor. Reprinted from ref. 154. Copyright from 2012 Royal Society of Chemistry.

influenza antibody. The detection was achieved within seconds, with a limit of detection of 3.67 pg ml^{-1}. This platform relies on electrical means to transport and detect target molecules, and the technology is compatible with external controls and readout circuitry for signal recording, processing and data transmission, which offers a new way for detecting low-abundance analytes in a timely manner.

3.3 Nuclear magnetic resonance (NMR)-based biosensor

NMR is a magnetic resonance-based sensing technology that has received considerable attention for the sensitive detection of biomolecule structures in recent years.[156] NMR is a phenomenon where the nuclei in a strong constant magnetic field are perturbed by a weak oscillating magnetic field which generates an electromagnetic signal with a frequency characteristic of the magnetic field at the nucleus. In an NMR-based biosensor, analytes that are labeled with magnetic particles are placed in a local magnetic field and are then excited by an NMR probe that consists of coils. The frequency of the excited nucleus pins is associated with the electron density of the analytes, and the electric current induced in the coil is recorded, followed by a Fourier transformation of the time domain signals. The resulting shifts in frequencies represent the unique chemical structures of detected biomolecules.[157] As the magnetic signals provided by nanometer sized magnetic particles are strong and can penetrate the opaque surrounding medium, micro-nuclear magnetic resonance (μNMR) can therefore detect various biomarkers in complex raw samples with minimal sample purification processes.[158,159] Nevertheless, the use of μNMR sensors still requires multi-step sample

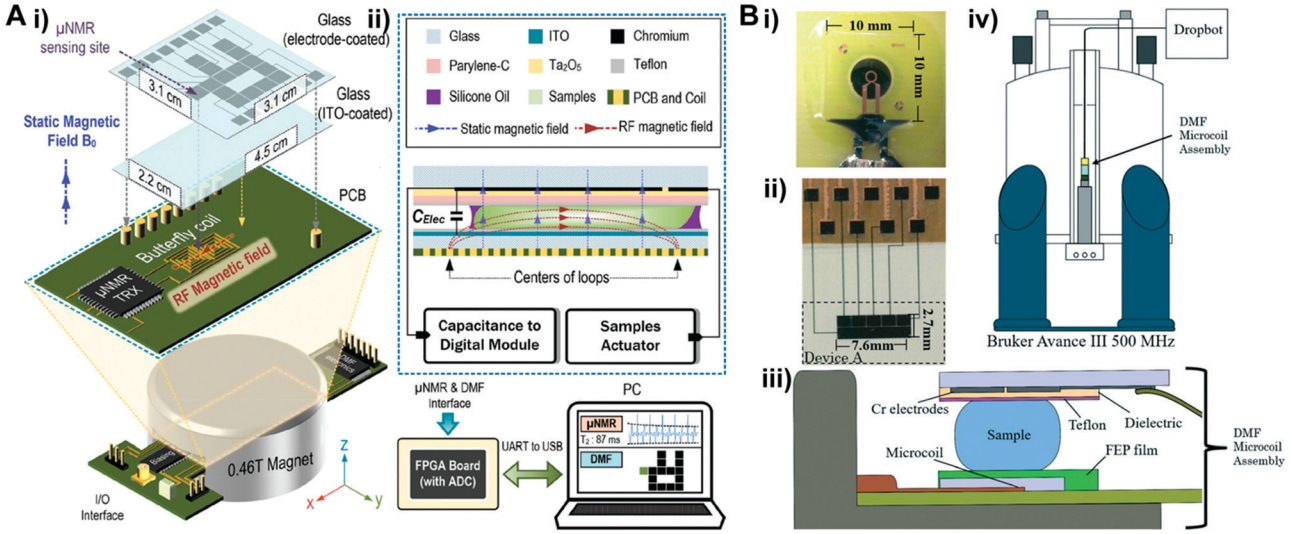

Fig. 9 (A) i) The diagram of a unified DMF device and micro-nuclear magnetic resonance (μNMR). A palm sized DMF device was assembled above a FPGA board containing butterfly coils. A permanent magnet was incorporated underneath the device to generate a static magnetic field, which is orthogonal to the RF magnetic field generated by the coils. ii) Cross-section of DMF and μNMR relaxometer interface. Both the sample actuator and capacitance-to-digital module were controlled by a FPGA board, which was connected to a computer for the visualizations of μNMR results and DMF control panel. Printed with permission from ref. 162. Copyright from 2015 Royal Society of Chemistry. (B) DMF–NMR i) photo of a Bruker planar microcoil; ii) photo of the top plate of a DMF device containing actuation electrodes and electrical contact pads; iii) cross-section diagram of the assembled DMF-microcoil; iv) schematic diagram of an integrated DMF system with a commercial high field NMR spectrometer. Printed with permission from ref. 163. Copyright from 2016 Royal Society of Chemistry.

preparation including probe labeling and sample transfer to the sensing sites. As sample preparation is an intrinsic, prominent strength of DMF platforms, the use of μNMR in DMF devices can allow automated sample processing and sensing at desired spots with reduced cross contamination and human intervention.

To integrate NMR into a DMF platform, it is essential to generate a magnetic field sufficiently strong (usually 1–20 tesla) within the device for sensitive spectroscopy.[160] To achieve this, Lei *et al.* interfaced a DMF device with a portable nuclear magnetic resonance relaxometer.[161,162] In this construct, a butterfly coil fabricated on a PCB board was sandwiched between a DMF chip and a portable magnet (Fig. 9A i), therefore the generated RF magnetic field intersected with the static magnetic field, forming a strong magnetic field inside of the DMF device (Fig. 9A ii). The μNMR relaxometers and DMF interface were controlled by a FPGA board linked to a computer for visualization and real-time monitoring. In this platform, avidin molecules were captured by immunomagnetic nanoparticles in a droplet and moved to a μNMR sensing site; as low as 0.2 μM avidin was quantified within 3 min.

Although this integrative and compact system can detect micromoles of biomolecules, the magnetic field generated by the μNMR is not sufficient for applications that require increased sensitivity, such as chemical structure analysis. In response to this limitation, Wheeler's group interfaced a DMF system with a commercial high field NMR spectrometer (Fig. 9) for chemical structure analysis that can identify chemical shifts related to, for example, protein conformation dynamics and diffusion kinetics.[163] In this interface, a Bruker planar microcoil (Fig. 9B i) was assembled underneath a single-plate DMF device (Fig. 9B ii and iii), and the assembly was vertically loaded into a spectrometer for characterization (Fig. 9B iv). In this configuration, droplets can be moved onto the microcoil surface, and reaction processes such as oxylose–borate complexation and glucose oxidase catalysis were analyzed based on NMR spectra captured at different time intervals. To enhance droplet manipulation, NMR-based sensors can also be integrated into two-plate DMF devices in which the top plate can house both the ground electrode for electrowetting and NMR microcoil,[164] and an additional protective insulating layer can ensure NMR measurement without compromising the droplet handling ability. A portable NMR–DMF platform as such that can generate a strong magnetic field is expected to unlock its potential in POC detection. Moreover, this system provides an improved spectral resolution and capability to handle more complicated chemical reactions including diffusion ordered spectroscopy and short-lived chemical reactions.[165] Despite these advantages, the sophisticated fabrication procedures still hinder the mass production of these chips. New fabrication strategies are needed for these platforms to be deployed in cost-effective, disposal POC tests.

3.4 Mass spectrometry

Mass spectrometry (MS) is a technology that analyzes the chemical elements of target species (*e.g.* proteins) based on the mass-to-charge ratio.[166] A mass spectrometer usually

comprises three parts: an ionizer, a mass analyzer and a detector. Samples injected into the ionizer vacuum tube are hit with electrons, and the ionized samples are then transferred to the mass analyzer under an electric field. A magnet in the mass analyzer will continuously bend the beam of ionized samples towards to the detector, during which ionized samples are sorted based on their mass-to-charge ratio. By recording the values of an indicator quantity on the detector, the abundance of each ion can be measured.[167] The coupling of MS and microfluidic platforms is challenging, since the micro/nanoscale volumes processed on-chip need to be transferred into a standard mass spectrometer. Despite the difficulties, efforts have been made to integrate microfluidic devices with different ionization methods including electrospray ionization (ESI) and matrix-assisted laser desorption ionization (MALDI). In MALDI, samples need to be dried and ionized prior to MS analysis; it is therefore challenging to integrate this technique into DMF platforms and are more often performed off-line.[168] Detailed reviews on sample preparation in DMF devices for MALID-MS can be found elsewhere.[8,168–171] In this section, we summarize efforts on integrating nESI/MALDI in DMF platforms which aims at transferring target samples directly into mass spectrometers for further processing.

In ESI, a high voltage is applied to a droplet of analytes, thus accumulating ions within the droplet to an area with a more intense electric field. When the electric force exceeds the surface tension force where the ions are accumulated, the sample droplet breaks into a stream of tiny droplets. Then, the solvent from these tiny droplets is evaporated, and the analytes become increasingly charged under strong electric field, eventually dissociating into a stream of charged ions for MS analysis.[172] Therefore, interfacing a DMF device with ESI-MS requires two key components: the emitter that generates tiny droplets and the high voltage to create an electric field strong enough for dissociation. Fig. 10 summarizes the emitters used to eject samples from DMF platforms for MS analysis, and their principles and advantages are included in Table 2.

Glass capillary emitters are a common type of emitters that rely on capillary forces to transport fluids, and are compatible with nESI-MS technology. In pioneering studies reported by Wheeler's group, a microchannel nano-electrospray emitter was coupled into a hybrid DMF platform to quantify amino acids from dried blood spots (DBS) to screen for metabolism disorder in newborns using in-line tandem MS analysis.[173–175] The integrated system consisted of multilayers for sample in-line processing: protein was

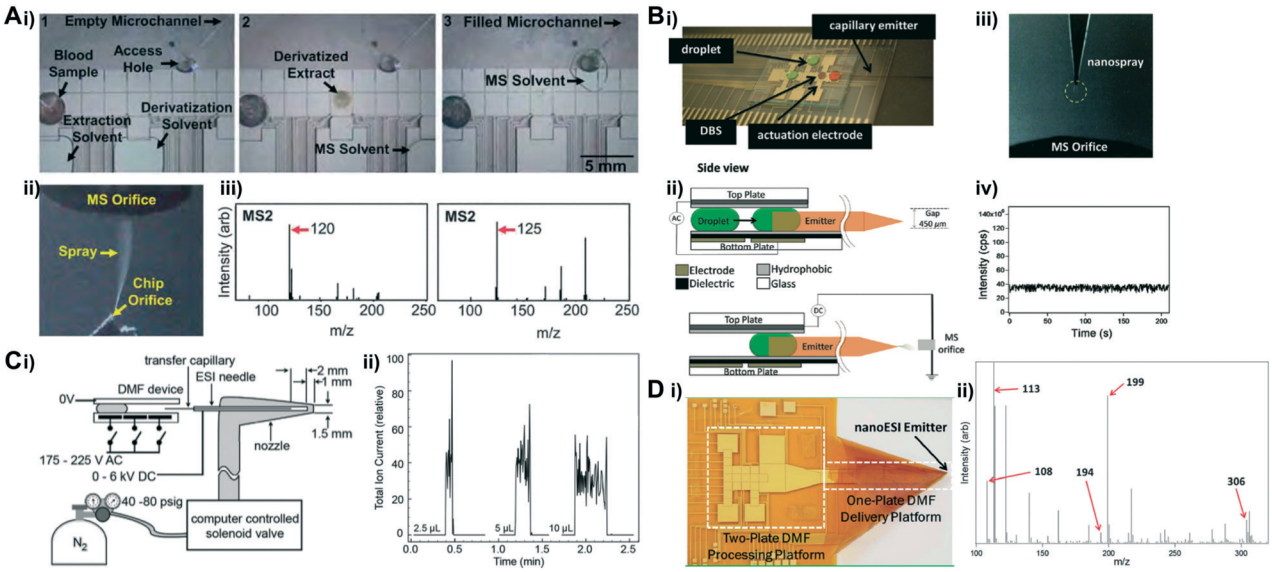

Fig. 10 (A) i) DMF for in-line MS analysis. Droplets were introduced through a dried blood spot to 1) extract amino acids (AA) from the dried blood spot (DBS), 2) resolubilize AA in solution and 3) move the analyte solution to the access hole with a spray microchannel for MS analysis. ii) Image of a sample spraying from an integrated nanoESI emitter. iii) Representative images of nESI-MS/MS spectra of amino acid Phe (*m*/*z* 120) (left) and d5-Phe (*m*/*z* 125) (right) obtained from DBS samples. Reprinted from ref. 173. Copyright from 2011 Royal Society of Chemistry. (B) i) Photo of a DMF device configured with a capillary emitter; ii) side-view of the integrated DMF-nESI-MS device. An AC electrical potential is generated between two plates to actuate droplets in the DMF device, and an DC bias is applied between the top substrate of the DMF device and the MS orifice to generate a nanoelectrospray; iii) image of a table spray generated at the tip of the capillary emitter; iv) total ion count as a function of time from a 15 μL droplet of tyrosine (5 μM). The spray was stable for >200 s, with an RSD of 7.3%. Reprinted from ref. 176. Copyright from 2012 American Chemical Society; C) i) a schematic representation of the eductor including a transfer capillary, ESI needle, and gas nozzle; ii) selected ion current traces when MRFA peptide droplets of 2.5 μL, 5 μL and 10 μL, were transferred from a DMF device to the MS *via* the eductor interface. Reprinted from ref. 178. Copyright from 2012 American Chemical Society; (D) i) photo of the microfluidic origami. The device includes a two-plate DMF device for processing droplets and a one-plate device to delivery droplets to the nanoESI emitter for in-line ESI MS analysis; ii) a representative mass spectrum demonstrating the Morita–Baylis–Hillman (MBH) reaction performed on the device. Reprinted from ref. 179. Copyright from 2011 Royal Society of Chemistry.

Table 2 Summary of technologies used for integrating a sample transfer system into DMF for in-line MS analysis

Technologies used to eject sample	Principles	Advantages	Ref.
Glass capillary emitter	Capillary force	Easy to fabricate, capable to work with nano-electrospray ionization mass spectrometry	173–177
Eductor interface	Bernoulli's principle	Rapid and continuous detection, low sample volume (<1 μL) required	178
Folded emitter	Bending a conical shaped orifice to transfer analytes	Cost-effective, disposable, suitable on flexible film	179

digested in the microchannels on the bottom layer and droplets were manipulated on the middle/top layer.[175] A blood drop was spotted on a filter paper in the DMF device, and the analytes were extracted through the filter paper (Fig. 10A i). The derivatized extract was then driven to the access hole and filled in the microchannel *via* capillary force and reached the ESI tip at the corner of the chip, and emitters sprayed the sample in the microchannel into the MS orifice (Fig. 10A ii). The MS analysis presented over 80% of sample recovery rate of amino acids in the DMF platform.

To increase the efficiency of sample dissociation and ionization, it is necessary to form droplets of smaller volumes. For this reason, a nanospray ESI (nESI) system was integrated into the DMF platform, where a pulled-glass capillary was placed between two DMF substrates with the nanosized taper end facing outward as the electrospray emitter to generate smaller droplets (Fig. 10B), allowing more effective dissociation and ion formation.[176,180] Droplets containing target analytes in DBS samples were manipulated to fill the emitter by capillary action for MS analysis. Additionally, the platform also integrated an impedance-based feedback control system to track the position of droplets in real-time. This nESI-MS platform was adopted to perform on-chip extraction and detection of succinylacetone (a marker of hepatorenal tyrosinemia) from DBS, and presented a comparable performance with standard techniques used in Newborn Screening Ontario (NSO). This platform was further extended for multiplexed testing, and parallel quantification of drugs of abuse from dried urine samples,[177] and can detect as low as 40 ng mL^{-1} cocaine in <15 min, which is >7× sensitive than the conventional immunoassay. The portable autonomous tandem MS holds great promise for fast and screening in DBS and other complex samples in POC applications as well as forensic testing.

Besides glass capillary emitters, Baker *et al.* developed an eductor interface composed of a fused silica transfer capillary coupled to a standard ESI needle for in-line MS analysis (Fig. 10C).[178] One of the transfer capillaries was placed between the two plates of a DMF device, while the other end was inserted into a standard ESI in a tapered gas nozzle. A pressure difference was formed at the outlet of the ESI needle as N_2 gas flowed through the nozzle *via* the Venturi effect, so that droplets on DMF were able to be pulled and transferred from the transfer capillary to the ESI needle for analysis. Different from the previously reported ESI-MS-DMF system, this system was able to decouple the spray DC voltage from the DMF actuation AC voltages, allowing continuous droplet delivery while conducting electrospray and MS analysis.

To reduce the cost for mass producing these devices as POC tests, attempts have been made to integrate MS technology into DMF devices built on flexible substrates. Kirby *et al.* integrated a folded nESI emitter[181] into a DMF platform on a non-planar flexible polyimide film substrate which formed a "microfluidic origami" for in-line analysis by MS (Fig. 10D).[179] The DMF platform combined both single and double plate configurations, and micro reactions occurred between two substrates and the droplets were then delivered onto the single plate for further processing. Conical shaped nESI emitters were formed by folding the single-plate interface with a 50 μm orifice, so that in-line MS analysis can be performed after droplets were delivered to the orifice at the cone apex. This system presented a capability for real-time analysis by performing the Morita–Baylis–Hillman (MBH) reaction and monitoring the reaction process by MS analysis. Compared with the widely used pulled glass capillary emitters (~$500 each), this folded polyimide emitter presented comparable detection performance at a low cost ($0.07) suitable for disposable use.

4. Conclusions

This review focuses on the integration of biochemical detection technologies into DMF devices, which can serve as a guide for future advancement toward POC applications. To date, optical, electrical, nuclear magnetic resonance and mass spectrometric techniques have been engaged in such integration, and presented highly sensitive and selective detection of enzymes, proteins, cells and nucleic acids, holding significant promise for POC diagnosis.

Currently, the major obstacles in integrating various detection mechanisms into DMF platforms are the need for bulky and specialized detection systems typically found in laboratory settings and the complex and costly device fabrication. Optical technology, as one of the most developed detection strategies with high sensitivity and selectivity, has already been implemented in commercial products but relies on bulky instruments. To overcome this hurdle, further efforts should focus on the miniaturization and full integration of DMF into portable optical platforms. The usage of compact optical instrumentation including LEDs and PMTs shows a

trend toward system miniaturization. In addition, as personal electronics and imaging devices continue to advance, smartphones can revolutionize healthcare due to the high-quality camera lenses and powerful imaging processing software. The customized app can also provide step-by-step instruction visually, bringing various screening tests from labs to homes. Besides, personal electronics can also be a promising detector of electrical signals since it is equipped with most of the major components including a battery for power supply, a processor for signal processing and a display screen.[182] Meanwhile, electrodes can be easily integrated into DMF devices, making electrical-based detection a promising option. However, the major concerns of such integration are the stability and reproducibility of the system, as well as the specificity[183] especially when detecting targets from complex sample fluids. In terms of MS, it provides unique information regarding chemical elements of the target sample, which makes it hard to be replaced by other technologies. Currently, the full integration between this technology and DMF cannot be readily miniaturized for POC diagnosis, but attempts to interface DMF devices with the mass analyzers for direct sample transfer with minimal sample loss and contamination are still worthwhile.

More often, most DMF devices are still fabricated in cleanroom settings, which require costly processes that largely limit their uses for POC applications. To overcome this hurdle, new trends are geared toward building the devices on inexpensive substrates. PCB, as a promising candidate, features advantages such as low cost for mass production and is often easy to integrate with electrical interfaces.[184] The prospering PCB manufacturing industries along with the various selection of electrode materials (*e.g.* nanotubes,[185] metal nanoparticles[186]) allow the customization of sensors with improved sensitivity, and further facilitate the adoption of the sensors to the market. Flexible substrates also present a new trend for integrative DMF devices, which include a polyester (PET) membrane[68] and paper.[67,187] These substrates are economical and disposable, more importantly, they are compatible with various commercial inkjet printers to print conductive silver/carbon nanotube electrodes. However, inkjet printing offers limited resolution. Alternative printing technologies such as electrohydrodynamic jet printing offer higher resolution, and can be used to form the actuation electrodes on one side of a paper substrate and electrical connection lines on the other.[75] Apart from its cost-effectiveness, this method also offers a promising way to alleviate a critical challenge in DMF device scaling due to the lack of practicality to accommodate larger arrays of electrodes and connection lines within several square inches. With the advancement in micro/nanofabrication technology, it would be possible to unlock the potential of deploying various integrative DMF devices for POC testing.

Conflicts of interest

There are no conflicts to declare.

Acknowledgements

This work was supported by the Ivan Bowen Family Foundation. In addition, we thank the Department of Surgery, the Microbiome Program, and the Center for Individualized Medicine at the Mayo Clinic for their support.

References

1 S. K. Vashist, *Biosensors*, 2017, **7**, 62.
2 K.-i. Ohno, K. Tachikawa and A. Manz, *Electrophoresis*, 2008, **29**, 4443–4453.
3 P. S. Dittrich, K. Tachikawa and A. Manz, *Anal. Chem.*, 2006, **78**, 3887–3908.
4 S. Haeberle and R. Zengerle, *Lab Chip*, 2007, **7**, 1094–1110.
5 K. Choi, A. H. C. Ng, R. Fobel and A. R. Wheeler, *Annu. Rev. Anal. Chem.*, 2012, **5**, 413–440.
6 M. Abdelgawad and A. R. Wheeler, *Adv. Mater.*, 2009, **21**, 920–925.
7 A. R. Wheeler, *Science*, 2008, **322**, 539–540.
8 M. J. Jebrail and A. R. Wheeler, *Curr. Opin. Chem. Biol.*, 2010, **14**, 574–581.
9 A. Banerjee, J. H. Noh, Y. Liu, P. D. Rack and I. Papautsky, *Micromachines*, 2015, **6**, 172–185.
10 A. Banerjee, Y. Liu, J. Heikenfeld and I. Papautsky, *Lab Chip*, 2012, **12**, 5138–5141.
11 R. B. Fair, *Microfluid. Nanofluid.*, 2007, **3**, 245–281.
12 T. M. Squires and S. R. Quake, *Rev. Mod. Phys.*, 2005, **77**, 977–1026.
13 Y. Liu, A. Banerjee and I. Papautsky, *Microfluid. Nanofluid.*, 2014, **17**, 295–303.
14 V. B. Kothamachu, S. Zaini and F. Muffatto, *SLAS Technol.*, 2020, **25**, 411–426.
15 S. L. S. Freire, *Sens. Actuators, A*, 2016, **250**, 15–28.
16 H. Kim, M. J. Jebrail, A. Sinha, Z. W. Bent, O. D. Solberg, K. P. Williams, S. A. Langevin, R. F. Renzi, J. L. Van De Vreugde, R. J. Meagher, J. S. Schoeniger, T. W. Lane, S. S. Branda, M. S. Bartsch and K. D. Patel, *PLoS One*, 2013, **8**, e68988.
17 H. Kim, M. S. Bartsch, R. F. Renzi, J. He, J. L. Van de Vreugde, M. R. Claudnic and K. D. Patel, *J. Lab. Autom.*, 2011, **16**, 405–414.
18 B. Coelho, B. Veigas, E. Fortunato, R. Martins, H. Águas, R. Igreja and P. V. Baptista, *Sensors*, 2017, **17**(7), 1495.
19 X. Xu, Q. Zhang, J. Song, Q. Ruan, W. Ruan, Y. Chen, J. Yang, X. Zhang, Y. Song, Z. Zhu and C. Yang, *Anal. Chem.*, 2020, **92**, 8599–8606.
20 Y. Liu, P. Jeraldo, H. Mendes-Soares, T. Masters, A. E. Asangba, H. Nelson, R. Patel, N. Chia and M. Walther-Antonio, *ACS Omega*, 2021, **6**, 25642–25651.
21 B. Seale, C. Lam, D. G. Rackus, M. D. Chamberlain, C. Liu and A. R. Wheeler, *Anal. Chem.*, 2016, **88**, 10223–10230.
22 **https://nanoporetech.com/prepare**.
23 **https://emea.illumina.com/company/news-center/press-releases/2015/2018793.html**.
24 J. Li and C.-J. C. Kim, *Lab Chip*, 2020, **20**, 1705–1712.

25 E. Samiei and M. Hoorfar, in *Miniature Fluidic Devices for Rapid Biological Detection*, ed. S.-H. Oh, C. Escobedo and A. G. Brolo, Springer International Publishing, Cham, 2018, pp. 171–205, DOI: 10.1007/978-3-319-64747-0_7.
26 https://www.genmarkdx.com/panels/eplex-panels/respiratory-pathogen-panel/.
27 https://www.genmarkdx.com/panels/eplex-panels/bcid-panels/.
28 https://www.genmarkdx.com/detection-of-variant-sars-cov-2-strains-on-eplex-rp2-panel/.
29 D. Millington, S. Norton, R. Singh, R. Sista, V. Srinivasan and V. Pamula, *Expert Rev. Mol. Diagn.*, 2018, **18**, 701–712.
30 X. Ding, P. Li, S.-C. S. Lin, Z. S. Stratton, N. Nama, F. Guo, D. Slotcavage, X. Mao, J. Shi, F. Costanzo and T. J. Huang, *Lab Chip*, 2013, **13**, 3626–3649.
31 R. J. Shilton, M. Travagliati, F. Beltram and M. Cecchini, *Adv. Mater.*, 2014, **26**, 4941–4946.
32 S.-K. Fan, T.-H. Hsieh and D.-Y. Lin, *Lab Chip*, 2009, **9**, 1236–1242.
33 O. D. Velev, B. G. Prevo and K. H. Bhatt, *Nature*, 2003, **426**, 515–516.
34 Y. Zhang and N.-T. Nguyen, *Lab Chip*, 2017, **17**, 994–1008.
35 U. Lehmann, S. Hadjidj, V. K. Parashar, C. Vandevyver, A. Rida and M. A. Gijs, *Sens. Actuators, B*, 2006, **117**, 457–463.
36 N.-T. Nguyen, M. Hejazian, C. H. Ooi and N. Kashaninejad, *Micromachines*, 2017, **8**(6), 186.
37 K. Joshi, V. Velasco and R. Esfandyarpour, *Sensors*, 2020, **20**, 3593.
38 G. Lippmann, *Ann. Chim. Phys.*, 1875, **5**(11), 494–549.
39 F. Mugele and J.-C. Baret, *J. Phys.: Condens. Matter*, 2005, **17**, R705.
40 B. Berge, *C. R. Acad. Sci., Ser. II: Mec., Phys., Chim., Sci. Terre Univers*, 1993, **317**, 157–163.
41 M. G. Pollack, A. D. Shenderov and R. B. Fair, *Lab Chip*, 2002, **2**, 96–101.
42 S. K. Cho, H. Moon and C.-J. Kim, *J. Microelectromech. Syst.*, 2003, **12**, 70–80.
43 J. Berthier, P. Dubois, P. Clementz, P. Claustre, C. Peponnet and Y. Fouillet, *Sens. Actuators, A*, 2007, **134**, 471–479.
44 W. C. Nelson and C.-J. C. Kim, *J. Adhes. Sci. Technol.*, 2012, **26**, 1747–1771.
45 P. Damborský, J. Švitel and J. Katrlík, *Essays Biochem.*, 2016, **60**, 91–100.
46 C. Chen and J. Wang, *Analyst*, 2020, **145**, 1605–1628.
47 E. M. Miller and A. R. Wheeler, *Anal. Chem.*, 2008, **80**, 1614–1619.
48 N. Vergauwe, D. Witters, F. Ceyssens, S. Vermeir, B. Verbruggen, R. Puers and J. Lammertyn, *J. Micromech. Microeng.*, 2011, **21**, 054026.
49 I. Barbulovic-Nad, H. Yang, P. S. Park and A. R. Wheeler, *Lab Chip*, 2008, **8**, 519–526.
50 Y. Wang, H. Zhao, X. Liu, W. Lin, Y. Jiang, J. Li, Q. Zhang and G. Zheng, *Biotechnol. Bioeng.*, 2021, **118**, 294–304.
51 B. B. Li, E. Y. Scott, M. D. Chamberlain, B. T. Duong, S. Zhang, S. J. Done and A. R. Wheeler, *Sci. Adv.*, 2020, **6**, eaba9589.
52 E. Moazami, J. M. Perry, G. Soffer, M. C. Husser and S. C. C. Shih, *Anal. Chem.*, 2019, **91**, 5159–5168.
53 E. M. Miller, A. H. C. Ng, U. Uddayasankar and A. R. Wheeler, *Anal. Bioanal. Chem.*, 2011, **399**, 337–345.
54 S. Kalsi, M. Valiadi, M.-N. Tsaloglou, L. Parry-Jones, A. Jacobs, R. Watson, C. Turner, R. Amos, B. Hadwen, J. Buse, C. Brown, M. Sutton and H. Morgan, *Lab Chip*, 2015, **15**, 3065–3075.
55 M. N. Tsaloglou, R. J. Watson, C. M. Rushworth, Y. Zhao, X. Niu, J. M. Sutton and H. Morgan, *Analyst*, 2015, **140**, 258–264.
56 S. Kalsi, S. L. Sellars, C. Turner, J. M. Sutton and H. Morgan, *Micromachines*, 2017, **8**(4), 111.
57 L. Wan, T. Chen, J. Gao, C. Dong, A. H.-H. Wong, Y. Jia, P.-I. Mak, C.-X. Deng and R. P. Martins, *Sci. Rep.*, 2017, **7**, 14586.
58 A. H. C. Ng, M. D. Chamberlain, H. Situ, V. Lee and A. R. Wheeler, *Nat. Commun.*, 2015, **6**, 7513.
59 J. Lamanna, E. Y. Scott, H. S. Edwards, M. D. Chamberlain, M. D. M. Dryden, J. Peng, B. Mair, A. Lee, C. Chan, A. A. Sklavounos, A. Heffernan, F. Abbas, C. Lam, M. E. Olson, J. Moffat and A. R. Wheeler, *Nat. Commun.*, 2020, **11**, 5632.
60 Q. Ruan, F. Zou, Y. Wang, Y. Zhang, X. Xu, X. Lin, T. Tian, H. Zhang, L. Zhou, Z. Zhu and C. Yang, *ACS Appl. Mater. Interfaces*, 2021, **13**, 8042–8048.
61 F. Zou, Q. Ruan, X. Lin, M. Zhang, Y. Song, L. Zhou, Z. Zhu, S. Lin, W. Wang and C. J. Yang, *Biosens. Bioelectron.*, 2019, **126**, 551–557.
62 R. S. Sista, A. E. Eckhardt, V. Srinivasan, M. G. Pollack, S. Palanki and V. K. Pamula, *Lab Chip*, 2008, **8**, 2188–2196.
63 R. Sista, Z. Hua, P. Thwar, A. Sudarsan, V. Srinivasan, A. Eckhardt, M. Pollack and V. Pamula, *Lab Chip*, 2008, **8**, 2091–2104.
64 X. Zeng, K. Zhang, J. Pan, G. Chen, A.-Q. Liu, S.-K. Fan and J. Zhou, *Lab Chip*, 2013, **13**, 2714–2720.
65 L. Coudron, M. B. McDonnell, I. Munro, D. K. McCluskey, I. D. Johnston, C. K. L. Tan and M. C. Tracey, *Biosens. Bioelectron.*, 2019, **128**, 52–60.
66 K. Choi, A. H. C. Ng, R. Fobel, D. A. Chang-Yen, L. E. Yarnell, E. L. Pearson, C. M. Oleksak, A. T. Fischer, R. P. Luoma, J. M. Robinson, J. Audet and A. R. Wheeler, *Anal. Chem.*, 2013, **85**, 9638–9646.
67 R. Fobel, A. E. Kirby, A. H. C. Ng, R. R. Farnood and A. R. Wheeler, *Adv. Mater.*, 2014, **26**, 2838–2843.
68 A. H. C. Ng, R. Fobel, C. Fobel, J. Lamanna, D. G. Rackus, A. Summers, C. Dixon, M. D. M. Dryden, C. Lam, M. Ho, N. S. Mufti, V. Lee, M. A. M. Asri, E. A. Sykes, M. D. Chamberlain, R. Joseph, M. Ope, H. M. Scobie, A. Knipes, P. A. Rota, N. Marano, P. M. Chege, M. Njuguna, R. Nzunza, N. Kisangau, J. Kiogora, M. Karuingi, J. W. Burton, P. Borus, E. Lam and A. R. Wheeler, *Sci. Transl. Med.*, 2018, **10**, eaar6076.
69 C. Dixon, J. Lamanna and A. R. Wheeler, *Lab Chip*, 2020, **20**, 1845–1855.
70 M. H. Shamsi, K. Choi, A. H. C. Ng, M. D. Chamberlain and A. R. Wheeler, *Biosens. Bioelectron.*, 2016, **77**, 845–852.

71 V. Rastogi and O. D. Velev, *Biomicrofluidics*, 2007, **1**, 014107.
72 V. Srinivasan, V. K. Pamula and R. B. Fair, *Lab Chip*, 2004, **4**, 310–315.
73 V. Srinivasan, V. K. Pamula and R. B. Fair, *Anal. Chim. Acta*, 2004, **507**, 145–150.
74 C. Peng, Z. Zhang, C.-J. C. Kim and Y. S. Ju, *Lab Chip*, 2014, **14**, 1117–1122.
75 A. T. Jafry, H. Lee, A. P. Tenggara, H. Lim, Y. Moon, S.-H. Kim, Y. Lee, S.-M. Kim, S. Park, D. Byun and J. Lee, *Sens. Actuators, B*, 2019, **282**, 831–837.
76 A. Abadian, S. S. Manesh and S. J. Ashtiani, *Microfluid. Nanofluid.*, 2017, **21**, 65.
77 S. H. Au, S. C. C. Shih and A. R. Wheeler, *Biomed. Microdevices*, 2011, **13**, 41–50.
78 Y. Wang, Q. Ruan, Z.-C. Lei, S.-C. Lin, Z. Zhu, L. Zhou and C. Yang, *Anal. Chem.*, 2018, **90**, 5224–5231.
79 L. Malic, T. Veres and M. Tabrizian, *Biosens. Bioelectron.*, 2009, **24**, 2218–2224.
80 L. Malic, T. Veres and M. Tabrizian, *Lab Chip*, 2009, **9**, 473–475.
81 L. Malic, T. Veres and M. Tabrizian, *Biosens. Bioelectron.*, 2011, **26**, 2053–2059.
82 C. Lerma Arce, D. Witters, R. Puers, J. Lammertyn and P. Bienstman, *Anal. Bioanal. Chem.*, 2012, **404**, 2887–2894.
83 S. F. Wondimu, S. von der Ecken, R. Ahrens, W. Freude, A. E. Guber and C. Koos, *Lab Chip*, 2017, **17**, 1740–1748.
84 F. Ceyssens, D. Witters, T. Van Grimbergen, K. Knez, J. Lammertyn and R. Puers, *Sens. Actuators, B*, 2013, **181**, 166–171.
85 S. H. Au, P. Kumar and A. R. Wheeler, *Langmuir*, 2011, **27**, 8586–8594.
86 V. N. Luk, G. C. H. Mo and A. R. Wheeler, *Langmuir*, 2008, **24**, 6382–6389.
87 X. Hou, Y. Hu, A. Grinthal, M. Khan and J. Aizenberg, *Nature*, 2015, **519**, 70–73.
88 D. C. Leslie, A. Waterhouse, J. B. Berthet, T. M. Valentin, A. L. Watters, A. Jain, P. Kim, B. D. Hatton, A. Nedder, K. Donovan, E. H. Super, C. Howell, C. P. Johnson, T. L. Vu, D. E. Bolgen, S. Rifai, A. R. Hansen, M. Aizenberg, M. Super, J. Aizenberg and D. E. Ingber, *Nat. Biotechnol.*, 2014, **32**, 1134–1140.
89 H. Geng and S. K. Cho, IEEE Micro Electro Mechanical Systems (MEMS), 21–25 Jan, 2018, pp. 261–264.
90 H. Geng and S. K. Cho, *Lab Chip*, 2019, **19**, 2275–2283.
91 A. G. Hadd, D. E. Raymond, J. W. Halliwell, S. C. Jacobson and J. M. Ramsey, *Anal. Chem.*, 1997, **69**, 3407–3412.
92 J. Pijuan, C. Barceló, D. F. Moreno, O. Maiques, P. Sisó, R. M. Marti, A. Macià and A. Panosa, *Front. Cell Dev. Biol.*, 2019, **7**, 107.
93 S. Tyagi and F. R. Kramer, *Nat. Biotechnol.*, 1996, **14**, 303–308.
94 L. J. Blum, S. M. Gautier and P. R. Coulet, *Anal. Lett.*, 1988, **21**, 717–726.
95 Y. Guan, in *Biosensors and Biodetection*, ed. A. Rasooly and K. E. Herold, Humana Press, Totowa, NJ, 2009, pp. 375–387, DOI: **10.1007/978-1-60327-567-5_21**.
96 L. Yang, M. Jin, P. Du, G. Chen, C. Zhang, J. Wang, F. Jin, H. Shao, Y. She, S. Wang, L. Zheng and J. Wang, *PLoS One*, 2015, **10**, e0131193.
97 Z. Zhang, J. Lai, K. Wu, X. Huang, S. Guo, L. Zhang and J. Liu, *Talanta*, 2018, **180**, 260–270.
98 Y. Wang, M. Wang, L. Han, Y. Zhao and A. Fan, *Talanta*, 2018, **182**, 523–528.
99 P. Zhang, Z. Lin, Y. Zhuo, R. Yuan and Y. Chai, *Anal. Chem.*, 2017, **89**, 1338–1345.
100 M. M. Richter, *Chem. Rev.*, 2004, **104**, 3003–3036.
101 S. Wang, L. Ge, Y. Zhang, X. Song, N. Li, S. Ge and J. Yu, *Lab Chip*, 2012, **12**, 4489–4498.
102 W. Miao, J. P. Choi and A. J. Bard, *J. Am. Chem. Soc.*, 2002, **124**, 14478–14485.
103 L.-M. Fu and Y.-N. Wang, *TrAC, Trends Anal. Chem.*, 2018, **107**, 196–211.
104 Z. Gu, M.-L. Wu, B.-Y. Yan, H.-F. Wang and C. Kong, *ACS Omega*, 2020, **5**, 11196–11201.
105 Z. Gu, J.-J. Luo, L.-W. Ding, B.-Y. Yan, J.-L. Zhou, J.-G. Wang, H.-F. Wang and C. Kong, *Micromachines*, 2021, **12**(11), 1423.
106 P. Kanitthamniyom, P. Y. Hon, A. Zhou, M. Y. Abdad, Z. Y. Leow, N. B. M. Yazid, V. L. W. Xun, S. Vasoo and Y. Zhang, *Microsyst. Nanoeng.*, 2021, **7**, 47.
107 Y. Liu and I. Papautsky, *Micromachines*, 2019, **10**(2), 107.
108 S. Zeng, D. Baillargeat, H.-P. Ho and K.-T. Yong, *Chem. Soc. Rev.*, 2014, **43**, 3426–3452.
109 P. Li, F. Long, W. Chen, J. Chen, P. K. Chu and H. Wang, *Curr. Opin. Biomed. Eng.*, 2020, **13**, 51–59.
110 B. Barbiellini, *Low Temp. Phys.*, 2017, **43**, 159–161.
111 T. Lee, J.-S. Wi, A. Oh, H.-K. Na, J. Lee, K. Lee, T. G. Lee and S. Haam, *Nanoscale*, 2018, **10**, 3680–3687.
112 X. X. Han, Y. Xie, B. Zhao and Y. Ozaki, *Anal. Chem.*, 2010, **82**, 4325–4328.
113 H. Chen, A. Das, L. Bi, N. Choi, J.-I. Moon, Y. Wu, S. Park and J. Choo, *Nanoscale*, 2020, **12**, 21560–21570.
114 E. Galopin, M. Beaugeois, B. Pinchemel, J.-C. Camart, M. Bouazaoui and V. Thomy, *Biosens. Bioelectron.*, 2007, **23**, 746–750.
115 Y. Huang, L. Zhang, H. Zhang, Y. Li, L. Liu, Y. Chen, X. Qiu and D. Yu, *Micromachines*, 2020, **11**(5), 526.
116 M. Trzaskowski, A. Napiórkowska, E. Augustynowicz-Kopeć and T. Ciach, *Sens. Actuators, B*, 2018, **260**, 786–792.
117 M. Baaske and F. Vollmer, *ChemPhysChem*, 2012, **13**, 427–436.
118 H. Abdullah, K. Ahmed and S. A. Mitu, *Results Phys.*, 2020, **17**, 103151.
119 K. D. Vos, I. Bartolozzi, E. Schacht, P. Bienstman and R. Baets, *Opt. Express*, 2007, **15**, 7610–7615.
120 S. I. Shopova, R. Rajmangal, S. Holler and S. Arnold, *Appl. Phys. Lett.*, 2011, **98**, 243104.
121 E. Kim, M. D. Baaske and F. Vollmer, *Lab Chip*, 2017, **17**, 1190–1205.
122 F. Vollmer and S. Arnold, *Nat. Methods*, 2008, **5**, 591–596.
123 N. Toropov, G. Cabello, M. P. Serrano, R. R. Gutha, M. Rafti and F. Vollmer, *Light: Sci. Appl.*, 2021, **10**, 42.
124 M. Hossein-Zadeh and K. J. Vahala, *Opt. Express*, 2006, **14**, 10800–10810.

125 M. Pöllinger, D. O'Shea, F. Warken and A. Rauschenbeutel, *Phys. Rev. Lett.*, 2009, **103**, 053901.
126 G. Chen, M. Jin, P. Du, C. Zhang, X. Cui, Y. Zhang, J. Wang, F. Jin, Y. She, H. Shao, S. Wang and L. Zheng, *Food Agric. Immunol.*, 2017, **28**, 315–327.
127 X. Fan, I. M. White, S. I. Shopova, H. Zhu, J. D. Suter and Y. Sun, *Anal. Chim. Acta*, 2008, **620**, 8–26.
128 N. J. Ronkainen, H. B. Halsall and W. R. Heineman, *Chem. Soc. Rev.*, 2010, **39**, 1747–1763.
129 T. Xu, Y. Song, W. Gao, T. Wu, L.-P. Xu, X. Zhang and S. Wang, *ACS Sens.*, 2018, **3**, 72–78.
130 D. Grieshaber, R. MacKenzie, J. Vörös and E. Reimhult, *Sensors*, 2008, **8**(3), 1400–1458.
131 Y. Yu, J. Chen, J. Li, S. Yang, S.-K. Fan and J. Zhou, *J. Micromech. Microeng.*, 2013, **23**, 095025.
132 M. D. M. Dryden, D. D. G. Rackus, M. H. Shamsi and A. R. Wheeler, *Anal. Chem.*, 2013, **85**, 8809–8816.
133 M. H. Shamsi, K. Choi, A. H. C. Ng and A. R. Wheeler, *Lab Chip*, 2014, **14**, 547–554.
134 Y. Yu, M. H. Shamsi, D. L. Krastev, M. D. Dryden, Y. Leung and A. R. Wheeler, *Lab Chip*, 2016, **16**, 543–552.
135 Y. Yu, R. P. S. de Campos, S. Hong, D. L. Krastev, S. Sadanand, Y. Leung and A. R. Wheeler, *Microsyst. Nanoeng.*, 2019, **5**, 10.
136 J. Das, K. B. Cederquist, A. A. Zaragoza, P. E. Lee, E. H. Sargent and S. O. Kelley, *Nat. Chem.*, 2012, **4**, 642–648.
137 D. G. Rackus, M. D. M. Dryden, J. Lamanna, A. Zaragoza, B. Lam, S. O. Kelley and A. R. Wheeler, *Lab Chip*, 2015, **15**, 3776–3784.
138 O. D. Renedo, M. A. Alonso-Lomillo and M. J. A. Martínez, *Talanta*, 2007, **73**, 202–219.
139 Z. Taleat, A. Khoshroo and M. Mazloum-Ardakani, *Microchim. Acta*, 2014, **181**, 865–891.
140 N.-B. Mincu, V. Lazar, D. Stan, C. M. Mihailescu, R. Iosub and A. L. Mateescu, *Diagnostics*, 2020, **10**(8), 517.
141 R. P. S. de Campos, D. G. Rackus, R. Shih, C. Zhao, X. Liu and A. R. Wheeler, *Anal. Chem.*, 2019, **91**, 2506–2515.
142 J. Gong and C.-J. C. Kim, *Lab Chip*, 2008, **8**, 898–906.
143 B. Hadwen, G. R. Broder, D. Morganti, A. Jacobs, C. Brown, J. R. Hector, Y. Kubota and H. Morgan, *Lab Chip*, 2012, **12**, 3305–3313.
144 K. Hu, B. Hsu, A. Madison, K. Chakrabarty and R. Fair, Des. Autom. Test Eur. Conf. Exhib. (DATE), 2013, 559–564.
145 C. Zhang, Y. Su, S. Hu, K. Jin, Y. Jie, W. Li, A. Nathan and H. Ma, *ACS Omega*, 2020, **5**, 5098–5104.
146 T. Lederer, S. Clara, B. Jakoby and W. Hilber, *Microsyst. Technol.*, 2012, **18**, 1163–1180.
147 S. O. P. Blume, R. Ben-Mrad and P. E. Sullivan, *Sens. Actuators, B*, 2015, **218**, 261–270.
148 E. Samiei, G. S. Luka, H. Najjaran and M. Hoorfar, *Biosens. Bioelectron.*, 2016, **81**, 480–486.
149 Y. Mashraei, S. Sivashankar, U. Buttner and K. N. Salama, *IEEE Sens. J.*, 2016, **16**, 8775–8783.
150 S. C. C. Shih, I. Barbulovic-Nad, X. Yang, R. Fobel and A. R. Wheeler, *Biosens. Bioelectron.*, 2013, **42**, 314–320.
151 D. Sung and J. Koo, *Biomed. Eng. Lett.*, 2021, **11**, 85–96.
152 L. Syedmoradi, A. Ahmadi, M. L. Norton and K. Omidfar, *Microchim. Acta*, 2019, **186**, 739.
153 N. N. Reddy and D. K. Panda, *Silicon*, 2021, **13**, 3085–3100.
154 K. Choi, J.-Y. Kim, J.-H. Ahn, J.-M. Choi, M. Im and Y.-K. Choi, *Lab Chip*, 2012, **12**, 1533–1539.
155 K. Choi, M. Im, J.-M. Choi and Y.-K. Choi, *Microfluid. Nanofluid.*, 2012, **12**, 821–827.
156 H. M. Rose, C. Witte, F. Rossella, S. Klippel, C. Freund and L. Schröder, *Proc. Natl. Acad. Sci. U. S. A.*, 2014, **111**, 11697.
157 P. Gillis and S. H. Koenig, *Magn. Reson. Med.*, 1987, **5**, 323–345.
158 H. Günther, *NMR spectroscopy: basic principles, concepts and applications in chemistry*, John Wiley & Sons, 2013.
159 Y. Luo and E. C. Alocilja, *J. Biol. Eng.*, 2017, **11**, 14.
160 R. M. Fratila and A. H. Velders, *Annu. Rev. Anal. Chem.*, 2011, **4**, 227–249.
161 K.-M. Lei, P.-I. Mak, M.-K. Law and R. P. Martins, *Analyst*, 2014, **139**, 6204–6213.
162 K.-M. Lei, P.-I. Mak, M.-K. Law and R. P. Martins, *Analyst*, 2015, **140**, 5129–5137.
163 I. Swyer, R. Soong, M. D. M. Dryden, M. Fey, W. E. Maas, A. Simpson and A. R. Wheeler, *Lab Chip*, 2016, **16**, 4424–4435.
164 I. Swyer, S. von der Ecken, B. Wu, A. Jenne, R. Soong, F. Vincent, D. Schmidig, T. Frei, F. Busse, H. J. Stronks, A. J. Simpson and A. R. Wheeler, *Lab Chip*, 2019, **19**, 641–653.
165 B. Wu, S. von der Ecken, I. Swyer, C. Li, A. Jenne, F. Vincent, D. Schmidig, T. Kuehn, A. Beck, F. Busse, H. Stronks, R. Soong, A. R. Wheeler and A. Simpson, *Angew. Chem., Int. Ed.*, 2019, **58**, 15372–15376.
166 B. Domon and R. Aebersold, *Science*, 2006, **312**, 212–217.
167 G. L. Glish and R. W. Vachet, *Nat. Rev. Drug Discovery*, 2003, **2**, 140–150.
168 A. E. Kirby and A. R. Wheeler, *Anal. Chem.*, 2013, **85**, 6178–6184.
169 X. Wang, L. Yi, N. Mukhitov, A. M. Schrell, R. Dhumpa and M. G. Roper, *J. Chromatogr. A*, 2015, **1382**, 98–116.
170 L. Malic, D. Brassard, T. Veres and M. Tabrizian, *Lab Chip*, 2010, **10**, 418–431.
171 N. S. Ha, M. de Raad and L. Z. Han, *RSC Chem. Biol.*, 2021, **2**(5), 1331–1351.
172 B. P. Pozniak and R. B. Cole, *J. Am. Soc. Mass Spectrom.*, 2007, **18**, 737–748.
173 M. J. Jebrail, H. Yang, J. M. Mudrik, N. M. Lafrenière, C. McRoberts, O. Y. Al-Dirbashi, L. Fisher, P. Chakraborty and A. R. Wheeler, *Lab Chip*, 2011, **11**, 3218–3224.
174 S. L. S. Freire, H. Yang and A. R. Wheeler, *Electrophoresis*, 2008, **29**, 1836–1843.
175 M. W. L. Watson, M. J. Jebrail and A. R. Wheeler, *Anal. Chem.*, 2010, **82**, 6680–6686.
176 S. C. C. Shih, H. Yang, M. J. Jebrail, R. Fobel, N. McIntosh, O. Y. Al-Dirbashi, P. Chakraborty and A. R. Wheeler, *Anal. Chem.*, 2012, **84**, 3731–3738.
177 A. E. Kirby, N. M. Lafrenière, B. Seale, P. I. Hendricks, R. G. Cooks and A. R. Wheeler, *Anal. Chem.*, 2014, **86**, 6121–6129.

178 C. A. Baker and M. G. Roper, *Anal. Chem.*, 2012, **84**, 2955–2960.
179 A. E. Kirby and A. R. Wheeler, *Lab Chip*, 2013, **13**, 2533–2540.
180 G. T. T. Gibson, S. M. Mugo and R. D. Oleschuk, *Mass Spectrom. Rev.*, 2009, **28**, 918–936.
181 A. E. Kirby, M. J. Jebrail, H. Yang and A. R. Wheeler, *Rapid Commun. Mass Spectrom.*, 2010, **24**, 3425–3431.
182 P. B. Lillehoj, M.-C. Huang, N. Truong and C.-M. Ho, *Lab Chip*, 2013, **13**, 2950–2955.
183 M. J. Russo, M. Han, P. E. Desroches, C. S. Manasa, J. Dennaoui, A. F. Quigley, R. M. I. Kapsa, S. E. Moulton, R. M. Guijt, G. W. Greene and S. M. Silva, *ACS Sens.*, 2021, **6**, 1482–1507.
184 R. Sista, Z. Hua, P. Thwar, A. Sudarsan, V. Srinivasan, A. Eckhardt, M. Pollack and V. Pamula, *Lab Chip*, 2008, **8**, 2091–2104.
185 M. Selvi, M. Rangaraj Vengatesan, P. Prabunathan, J. Kun Song and M. Alagar, *Appl. Phys. Lett.*, 2013, **103**, 152902.
186 M. Veerapandian, Y.-T. Seo, K. Yun and M.-H. Lee, *Biosens. Bioelectron.*, 2014, **58**, 200–204.
187 A. Abadian and S. Jafarabadi-ashtiani, *Microfluid. Nanofluid.*, 2014, **16**, 989–995.